Invited submission to
Annual Review of Fluid Mechanics

Designing Complex Fluids

Randy H. Ewoldt[a,b,*], Chaimongkol Saengow[b,**]

[a] Department of Mechanical Science and Engineering, University of Illinois at Urbana-Champaign, Urbana, Illinois 61801, USA
[b] Beckman Institute for Advanced Science and Technology, University of Illinois at Urbana-Champaign, Urbana, Illinois 61801, USA

* Corresponding author: Email: ewoldt@illinois.edu; ORCID: 0000-0003-2720-9712
** Email: saengow@illinois.edu; ORCID: 0000-0002-3869-5616

Shortened Running Title: **Designing Complex Fluids**

Keywords

rheology, design, constitutive models, microstructure, non-Newtonian fluids

Abstract

A small step away from Newtonian fluid behavior creates an explosion in the range of possibilities. Non-Newtonian fluid properties can achieve diverse flow objectives, but the complexity introduces challenges. We survey useful rheological complexity along with organizing principles and design methods as we consider: How can non-Newtonian properties be useful? What properties are needed? How can we get those properties?

1. INTRODUCTION

To be Newtonian is restrictive; to be non-Newtonian is everything else. The open canvas of rheological complexity allows us to imagine a vast range of possible non-Newtonian equations for the stress tensor $\underline{\underline{\sigma}}$ in the momentum equation

$$\rho \frac{D\underline{v}}{Dt} = \rho \underline{g} - \underline{\nabla} p + \underline{\nabla} \cdot \underline{\underline{\sigma}} \tag{1}$$

to achieve diverse objectives. The design freedom for $\underline{\underline{\sigma}}$ is immense, even if we limit ourselves to incompressible fluids for which $\underline{\nabla} \cdot \underline{v} = 0$. Whereas incompressible isotropic Newtonian behavior is universally governed by a single equation, $\underline{\underline{\sigma}} = \mu\left(\underline{\nabla}\underline{v} + (\underline{\nabla}\underline{v})^T\right)$, with viscosity μ, there is no single equation for all possible non-Newtonian behaviors (Alves et al. 2021; Bird 1976; Bird & Wiest 1995; Bird et al. 1987; Joseph 1990; Larson & Desai 2015a; Larson & Wei 2019; Mewis & Wagner 2012).

Rheological complexity facilitates engineering designs across a remarkable range of applications, including human health, energy, the environment, manufacturing, food, robotics, and beyond. Complex fluids are also critical in biological contexts such as animal survival strategies (Ruehs et al. 2021). For example, making a fluid shear-thinning rather than Newtonian can enable extrusion based additive manufacturing (Truby & Lewis 2016), injectable hydrogels that provide spatial and temporal control of drug delivery (Li & Mooney 2016), and wall-climbing robots inspired by snails (Ewoldt et al. 2007). Shear thinning is just one way to violate Newtonian fluid assumptions (Figure 1). The intention of this review is to survey the broad landscape of useful fluid complexity and to identify organizing principles and emergent methods that enable design of complex fluid properties.

Design is inherently an inverse problem: to achieve the desired result, many solutions may be available.[1] The inverse problem of design contrasts the forward problem of analysis. In complex fluids, analysis may focus on a single constitutive equation or single type of material (e.g. one of the microstructures in Figure 2) and try to understand what consequences result for rheology and flow. Design goes the other direction: starting with an objective for the flow, we ask what properties are needed, and which microstructures can achieve them. The design freedom includes the properties of the fluid itself: the possible constitutive behavior of $\underline{\underline{\sigma}}$, and the possibility of optimizing functions or parameters therein. Of course, reality must eventually constrain our dreaming to realizable fluid formulations. Thus, to design in the world of rheologically-complex fluid properties, we consider three questions:

How can non-Newtonian properties be useful?

What properties are needed?

How can we get those properties?

With these questions in mind, we survey useful rheological complexity and associated design methods; examples make the methods concrete and useful for creative uses of rheology not yet imagined.

2. PARADIGMS FOR RHEOLOGY AND DESIGN

2.1. Four key phenomena

Breaking the law of Newtonian viscosity happens in four main ways (Macosko 1994), as shown with flow scenarios in Figure 1: viscoelasticity, shear thinning, shear normal stresses, and

[1] We avoid the term "inverse design" because, if done right, design is already an inverse problem.

extensional thickening. For each, there is an associated rheological property shown below each image in Figure 1. Rheological properties are described by shapes of curves, known as material functions, rather than a Newtonian viscosity. The design perspective considers what shapes of these functions are needed to achieve an objective. Often this complexity is simplified to low-dimensional descriptions. For example, the linear viscoelastic stress relaxation modulus $G(t)$ can be characterized by plateau moduli and characteristic timescales, as with the longest timescale τ associated with the final decay of $G(t)$ in Figure 1, which rationalizes the conditions of bouncing for impact time $t < \tau$ versus flowing for times $t > \tau$. The other three phenomena are nonlinear, characterized by a critical flow strength to see the non-Newtonian effect, either in terms of shear stress σ, shear strain rate $\dot{\gamma}$, or extensional strain rate $\dot{\varepsilon}$. Measurements of these properties can be non-trivial (Macosko 1994), especially in extensional flow (McKinley & Sridhar 2002).

Other important rheological phenomena exist that are not explicitly named in Figure 1, notably shear thickening, yield-stress fluids, and thixotropy. These can all be related to the nonlinear viscous shear-thinning phenomena. Shear thickening is simply the opposite: an increase of shear viscosity with applied stress (Morris 2020). Yield-stress fluids can be considered an extreme example of shear thinning: at low stress the viscosity is so large that the material behaves effectively as a solid, though it flows at sufficiently high applied stress (Bonn et al. 2017; Nelson et al. 2019); the green fluid in Figure 1 approaches this limit of a yield-stress fluid. Thixotropy relates to time dependence of shear thinning: thixotropy is time-dependent decrease of viscosity at high flow strength, and subsequent time-dependent recovery at low flow strength (Larson & Wei 2019).

The four key phenomena are useful for pedagogy, and useful as a design perspective: for a given flow objective, which rheological property is most critical? And what features of the material function might be needed?

2.2. Dimensionless numbers

Dimensionless numbers help navigate different rheological complexities. Chief among them are the Deborah and Weissenberg numbers (Dealy 2010; Poole 2012). The Deborah number, $De \equiv \tau/t$, compares the viscoelastic relaxation time τ to the relevant flow timescale t. Larger values indicate the emergence and importance of elastic effects (e.g. the bouncing ball of fluid in Figure 1 is at high *De*). Nonlinear behaviors, including the other three phenomena in Figure 1, are dictated by flow strength A, which can be in terms of strain, strain rate, or stress (Ewoldt & McKinley 2017; Pipkin 1972). The Weissenberg number is the most common flow strength (Dealy 2010; Poole 2012), $Wi = \tau\dot{\gamma}$, where $\dot{\gamma}$ is a characteristic strain rate of the flow. A more general dimensionless flow strength would be $\dot{\gamma}/\dot{\gamma}_{crit}$, or a stress-based amplitude σ/σ_{crit}, where the subscript "crit" references a critical magnitude for emergence of significant nonlinear behavior (be it shear-thinning viscosity, shear normal stress, or extensional thickening). For some materials the nonlinear $\dot{\gamma}_{crit}$ is inversely related to the linear property τ, in particular when diffusive timescales set both the linear relaxation time and onset of nonlinearity, for which $\dot{\gamma}_{crit} \sim \tau^{-1}$ and $Wi = \tau\dot{\gamma}$ is used. The specific criteria of nonlinear elastic streamline tension is the basis of the more historic and narrower definition of *Wi* based on elastic tensile stresses (Poole 2012), $Wi = N_1/(2\sigma)$, which reduces to $Wi = \tau\dot{\gamma}$ only in special cases where nonlinear normal stress difference N_1 can be directly mapped to the linear viscoelastic time τ. This is not always the case; percolated colloidal

networks that break down in flow are a counterexample where N_1 may be small yet shear thinning dramatic, and a critical stress σ/σ_{crit} may be more useful to quantify nonlinear flow strength.

Deborah number and flow strength define a two-dimensional space known as a Pipkin map (Pipkin 1972), to organize viscoelasticity and nonlinearity. Flows can exist in different regions, revealing the importance (or not) of different rheological properties that can be exploited for the purpose of design (Corman & Ewoldt 2019; Schuh & Ewoldt 2019). A third dimension is needed for thixotropic effects (Ewoldt & McKinley 2017), as will be noted in Section 4.1.

2.3. Material Microstructures

Many material microstructures are available to produce each of the rheological phenomena of Figure 1. Figure 2 shows six important examples that involve polymers, particles, and droplets. When these materials are added into an existing fluid, they might be called rheological modifiers, and handbooks for these exist (Ash & Ash 2006; Braun & Rosen 2000) to support chemical formulation (Bröckel et al. 2013) and chemical product design (Cussler & Moggridge 2011). Several textbooks are available that explain, for a given material structure, what rheological properties might result, e.g. (Gauzzelli & Morris 2012; Graham 2018; Larson 1999; Rubinstein & Colby 2003). These are typically organized from the analysis perspective, i.e. the forward problem of cause and effect. Design-inspired thinking flips this perspective, changing the structure-to-rheology path to be the inverse problem of rheology-to-structures (note the plural).

2.4. Design Hierarchy

Complex fluid design involves chemistry, material building blocks, microstructure, properties, and flows (Corman et al. 2016; Nelson et al. 2019). The order of this list emphasizes the forward

problem of analysis, whereas the reverse order emphasizes the inverse problem of design for a targeted behavior. Beyond complex fluids, soft materials also involve this design hierarchy (Sherman et al. 2020). Design tasks involve both continuum-level and microstructural-level aspects (Corman et al. 2016; Nelson et al. 2019). Continuum-level approaches involve tensorial constitutive models to relate rheological properties to flow behavior (often with perspectives from Sections 2.1, 2.2). Microstructural-level approaches (with paradigms from Section 2.3) relate material chemistry and building blocks to the rheological properties. These two levels have been contrasted as "design with" versus "design of" complex fluids, respectively (Corman et al. 2016; Nelson et al. 2019). Our review will touch on both.

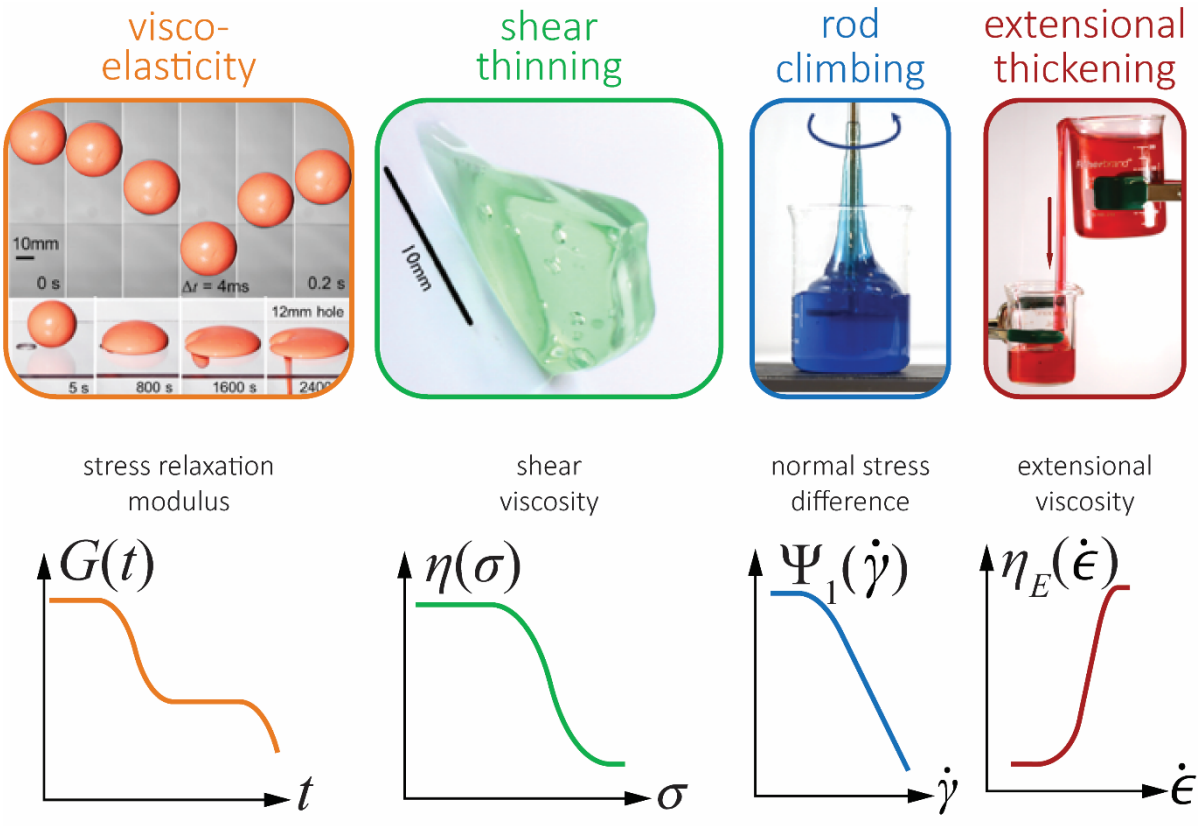

Figure 1: Four key rheological phenomena, connecting flow physics to the responsible rheological property (material function), each function schematic uses log scales. From left: viscoelasticity with bouncing and flowing therapy putty (similar to Silly Putty®); shear thinning viscosity with a semi-solid gel partially flowing down an incline (1wt% Carbopol in water); shear normal stresses cause rod climbing (2wt% PEO of $M_w \approx 8{\cdot}10^6$ g/mol in water); and extensional thickening causes emptying of the upper container via the open-siphon effect (2.2wt% polyacrylamide of $M_w \approx 5{\cdot}10^6$ g/mol in glycerol/water). The concepts of thixotropy and yield-stress fluids are subsets of the shear-thinning phenomenon. Images for viscoelasticity and shear thinning adapted from (Ewoldt 2014); remaining images from The Rheology Zoo at https://go.illinois.edu/4-Key-Phenom and Supplemental Videos 1-4.

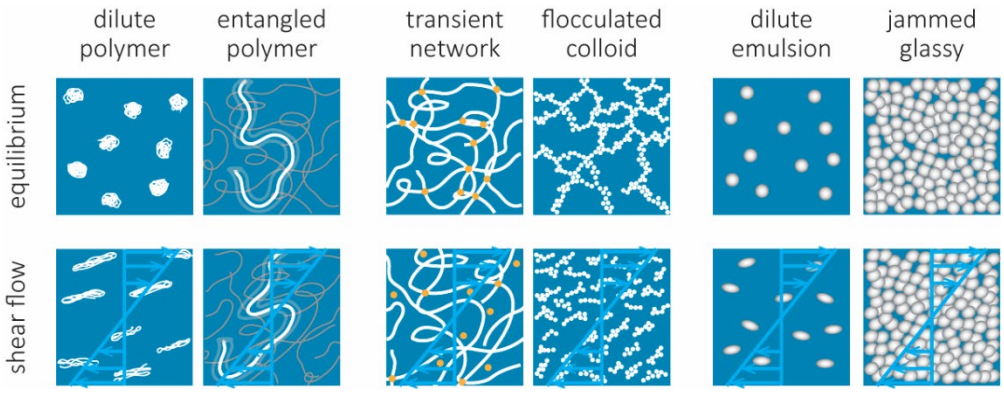

Figure 2: Many microstructures are available to create rheological complexity. Six important examples are shown, which involve polymers, particles, and droplets. The equilibrium structures (top row) are changed due to shear flow (bottom row) in different ways that may involve orientation, stretching, change of pair distribution functions, and breaking attractive connections. Most microstructures will show all the rheological phenomena noted in Figure 1, but to varying degrees of observability and importance. Schematics inspired by (Corman 2015).

3. USEFUL RHEOLOGICAL COMPLEXITY

We use the four key phenomena of Figure 1 to organize our survey of how complex fluids can be useful. This contrasts organization by material structure, i.e. listing applications separately for polymers, particles, droplets, etc. of Figure 2. Many different microstructures may achieve the target rheology. We recognize at the outset that we omit soft solids. Soft solids can be useful, e.g. for vibration dampening (Verbaan et al. 2017), mimicking vocal fold tissues (Zeitels et al. 2011), strain stiffening elastomers for mimicking tissues (Dobrynin & Carrillo 2011), or enhanced magnetorheological elastomers based on elastic strain stiffening (Chaudhary et al. 2020), but these are beyond our scope.

Every application considered here has a flow field, though of varying complexity. Complex velocity fields can make it difficult to isolate which rheological property in Figure 1 is most critical; simpler flow fields, close to either simple shear or uniaxial extension, more naturally isolate a primary property. Figure 3 is a perspective on complex flows versus complex fluids. Flow complexity may range from turbulence, where Newtonian fluids (Figure 3a1) can be made slightly

non-Newtonian to cause drag reduction (Figure 3a2), to the opposite extreme of simple velocity fields of steady laminar flow in a pressure driven channel (Figure 3d) where strong nonlinear shear thinning changes the parabolic profile to a plug-like profile with low shear rates to avoid damage to suspended cells. The complexity of the rheology also varies, from weak deviations from Newtonian behavior, which can explain the particle focusing in Figure 3b, to dramatically nonlinear yield-stress fluids used for the embedded droplet printing in Figure 3c. In what follows, we organize applications based on which of the key phenomena is primarily responsible (Figure 4), although many involve multiple properties.

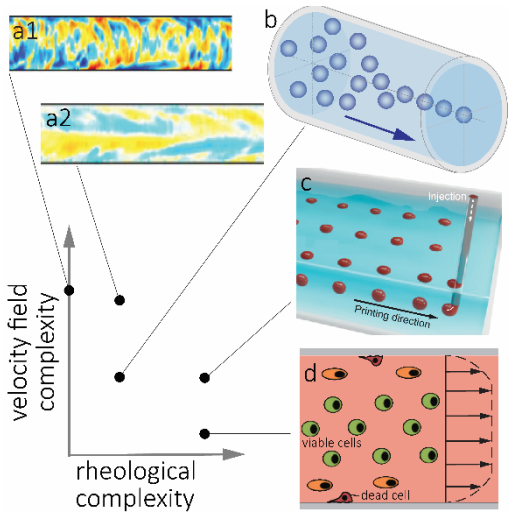

Figure 3: Useful non-Newtonian flows across a range of complexities (of velocity field and rheology): (a) turbulent drag reduction with dilute polymer solutions, (b) particle focusing due to shear normal stress effects, (c) embedded droplet printing in a yield-stress fluid, and (d) injection of cells with increased viability due to plug flow of a yield-stress fluid. Images in (a), (c), and (d) adapted with permission from (Choueiri et al. 2018; Nelson et al. 2020a), and (Blaeser et al. 2016), respectively.

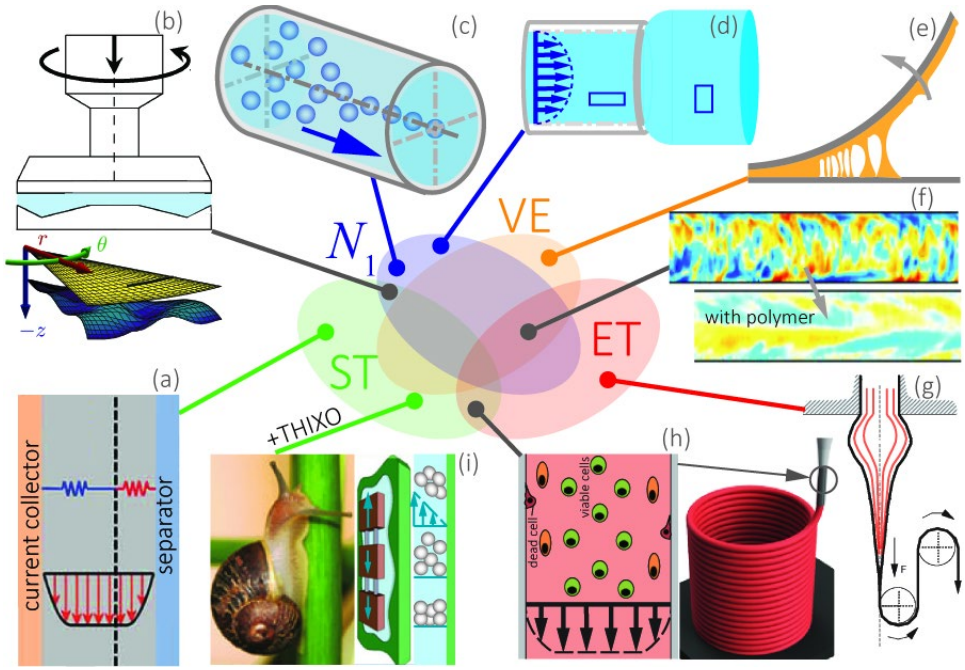

Figure 4: A selection of useful flow objectives, located on a Venn diagram of rheological phenomena based on what is most critical for the outcome: shear thinning (ST), normal stress in shear (N_1), linear viscoelasticity (VE), and extensional thickening (ET). Thixotropic breakdown and recovery (+THIXO) is indicated when relevant, but only exists within the context of shear thinning. Clockwise from bottom left: (a) flow battery, (b) thrust bearing, (c) particle focusing, (d) extrudate swell (a.k.a. die swell), (e) adhesion which can rely on linear or nonlinear viscoelasticity, (f) turbulent drag reduction, (g) fiber spinning, (h) direct-write printing with embedded cells, and (i) adhesive locomotion with snail-inspired robot. Images in (a), (f), and (g) are adapted with permission from, respectively, (Wei et al. 2015b), (Baird & Collias 2014; Choueiri et al. 2018).

3.1. Linear Viscoelasticity

Viscoelasticity involves elastic energy storage and loss, fluid memory, and time dependence, as in Figure 1. Many different rheological functions exist to characterize it (Bird et al. 1987). The relaxation modulus $G(t)$ quantifies time-dependent relaxation after imposed shear deformation, and its characteristic longest relaxation time τ is used in *De*. Oscillatory deformation can reveal decomposed storage and loss moduli, $G'(\omega)$ and $G''(\omega)$. The response to imposed step shear stress reveals the time-dependent creep compliance $J(t)$ and associated retardation timescales. All of these are interrelated in the limit of linear viscoelasticity (LVE) at small flow strength forcing: small stress, strain, and strain rates, e.g. Weissenberg number $Wi \ll 1$. In the absence of nonlinear

effects, the time-dependent effects can still be useful. This is especially true for energy dissipating elastomers (tires, shoes, machine mounts), but here we focus on viscoelastic fluids.

Viscoelastic fluids can be used for vibration dampening and shock absorption. Minimizing vibrations in skyscrapers, automotive transport, and spacecraft attitude control are a few examples (Corman 2019). The associated fluid flow may be simple (e.g. primarily shear in dashpot-style geometries) or more complex, but adding elasticity to the fluid involved is helpful for modifying transmission of forces and raises the question: what is the optimal shape of the viscoelastic response function? For incompressible linear viscoelasticity, the Boltzmann superposition equation governs all behavior, $\underline{\underline{\sigma}} = \int_{-\infty}^{t} G(t-t')\dot{\underline{\underline{\gamma}}}(t')dt'$ where $\dot{\underline{\underline{\gamma}}} = \underline{\nabla v} + (\underline{\nabla v})^T$ and the kernel function $G(t)$ is the stress relaxation modulus, which can be considered as the design freedom (Corman et al. 2016), whatever the chemistry and microstructure. For design purposes it can be represented with a continuous distribution of relaxation modes, $G(t) = \int_0^\infty \frac{H(\tau)}{\tau} e^{-t/\tau} d\tau$, where $H(\tau)$ is the viscosity-weighted continuous relaxation spectrum (Tschoegl 1989). Rheological design can be posed with $G(t)$ or $H(\tau)$ (Corman 2019), but assuming full design freedom of multiple LVE functions, e.g. both $G'(\omega)$ and $G''(\omega)$, violates the Kramers-Kronig interrelation and is therefore unallowable design freedom (Corman et al. 2016). In the works of (Corman 2019; Corman et al. 2016), design for vibration isolation was considered using a one-dimensional abstracted model of the fluid flow. The viscoelastic function was parameterized with realistic shapes describing typical behaviors and optimized with methods including multi-objective approaches that recognize tradeoffs, e.g. better handling versus better vibration isolation in a car suspension. A Pareto set of possible designs shows a family of targeted viscoelastic behavior, depending on the tradeoff preference.

How can the target shapes of viscoelastic functions be compared to realizable complex fluids? Low-dimensional representations have been suggested for the purpose of making Ashby plots (Ashby 2011) with viscoelastic fluid properties (Corman & Ewoldt 2019), as in Figure 5. Ashby-style plots have also been considered for other rheological properties, namely for yield-stress fluids (Ewoldt et al. 2007; Nelson et al. 2018). Similar plots and associated databases for other key rheological properties will accelerate future design efforts.

Adhesives often benefit from linear viscoelasticity and design targets have been expressed as low-dimensional features of linear viscoelastic functions. For pressure-sensitive adhesives (PSAs), linear viscoelastic criteria have been correlated with performance (Chang 1991; Creton & Ciccotti 2016; Dahlquist 1969; Dahlquist & Kolpe 1974; de Gennes 1996), including the Dahlquist criteria of sufficiently low elastic modulus (e.g. 10-100 kPa at 1 Hz) so that the material can conform to the substrate, and target ranges of (G',G'') (called Chang windows), evaluated at different frequencies, which indicate different dissipation ratios for different applications. There can also be a requirement of minimal creep, which can be achieved by crosslinking the material to be solid, or nearly so. These criteria are all based on simple features of otherwise function-valued viscoelastic properties, i.e. detailed shapes of $G'(\omega)$ and $G''(\omega)$ are not considered. PSAs are typically polymeric materials. The viscoelastic properties can be tuned to change the adhesive performance (Deplace et al. 2009) and the Chang Windows have been used to guide the design of triblock copolymers for renewable PSA applications (Ewert et al. 2018). Beyond linear viscoelasticity and PSAs, other adhesives may benefit from having yield-stress fluid behavior to provide grab strength before curing, and nonlinear viscoelastic behavior of extensional thickening which increases energy dissipation at large deformations (Christensen & McKinley 1998; Tripathi et al. 2000).

Locomotion at low Reynolds number is influenced by linear viscoelasticity (Fulford et al. 1998; Lauga 2014, 2016), but it can be difficult to isolate linear effects from nonlinear normal stress differences and extensional thickening. Studies with polymer solutions have indicated the importance of normal stress differences (Espinosa-Garcia et al. 2013; Puente-Velázquez et al. 2019). These works are primarily analysis, focused on cause and effect insight, but they lay the groundwork for possible inverse problem statements of design to ask for optimal rheology. This is a challenging task that will require concepts of co-design (Lee et al. 2019), since the microswimmer shape and locomotion kinematics (gait) also create design freedom that couples with the fluid rheology to result in locomotion.

It can be difficult to design within the strict confines of linear viscoelasticity since many flows will involve finite-amplitude effects. However, linear viscoelasticity is a starting point for nonlinear effects, and there are good predictive equations of τ for a wide range of microstructures (more detail in Section 4.2). In fact, we will see that design criteria for nonlinear effects are often framed in terms of the linear viscoelastic relaxation time τ, as suggested already by the use of $Wi = \tau\dot{\gamma}$ for fluid nonlinearity. But the reader is cautioned that such linear-to-nonlinear mappings are not universal across material structures (Figure 2), except in the limit of weak non-Newtonian behavior known as the Ordered Fluid Expansion (see sidebar titled Which Complexity Comes First?). The linear-to-nonlinear mapping can apply in strong flows for some special polymer systems (see sidebar titled Boger Fluid Design & Decoupled Rheology).

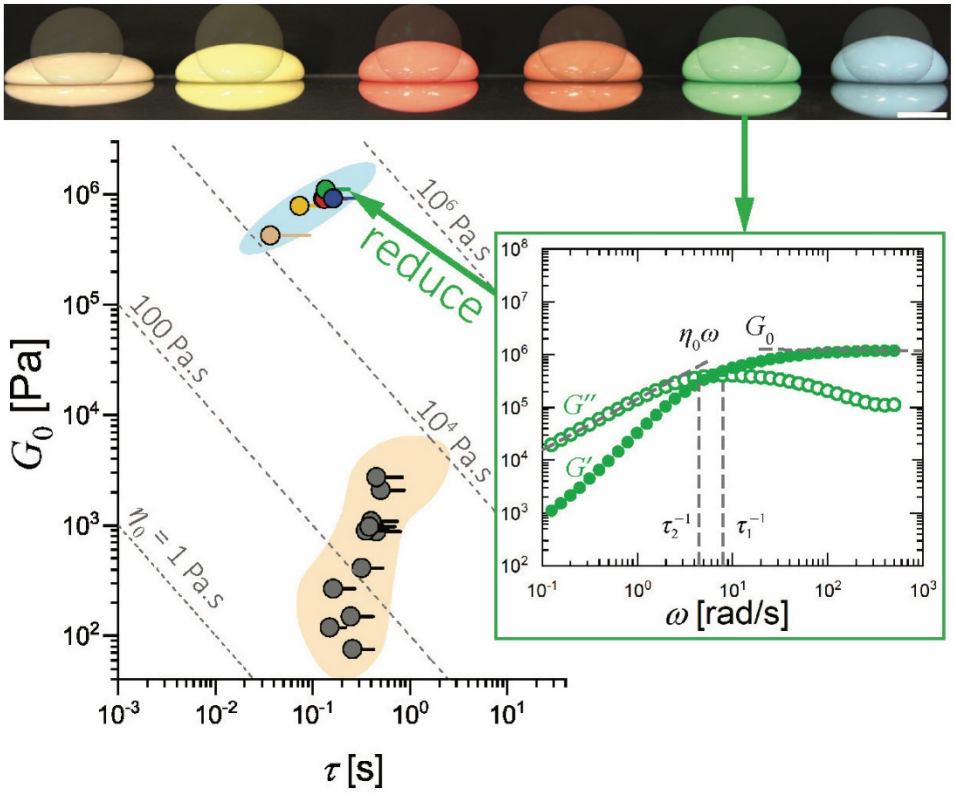

Figure 5: Ashby-style plot for linear viscoelastic fluids. Figure adapted with permission from (Corman & Ewoldt 2019). Data shown for therapy putties (similar to Silly Putty®), photos at top, and a range of transient polymer networks of PVA-Borax (gray). Each point collapses the viscoelastic relaxation function into a low-dimensional description. Points are located at (τ_1,G_0), with a tail extending to τ_2 to indicate the underlying continuous spectrum of relaxation times $H(\tau)$, where G_0 is the high frequency elastic modulus, τ_1 the first-moment average timescale, and τ_2 the second-moment average timescale. Steady shear viscosity is shown with η=$G_0\tau_1$ dashed lines.

WHICH COMPLEXITY COMES FIRST?

The smallest step beyond Newtonian behavior introduces slight viscoelasticity, shear normal stresses, and extensional thickening, all at the same order. This is the insight from the microstructure-agnostic perturbative expansion of a second-order fluid (Bird et al. 1987), which in simple shear predicts $N_1 = \Psi_1 \dot{\gamma}^2$ with constant Ψ_1, shear stress $\sigma = \eta\dot{\gamma}$ with constant η, and the linear-to-nonlinear mapping $\tau = \Psi_1/2\eta$. Shear thinning appears at third order and is thus more rheologically complex as suggested in Figure 3. When designing with dilute additives, N_1 and $\eta_E > 3\eta$ may be more important than shear thinning. Mathematically, the ordered fluid expansion

helps explain why N_1 and $\eta_E > 3\eta$ often appear together. Physically, this is because both involve tension along streamlines. This is easiest to understand with dilute polymers that stretch and orient in flow, but any microstructure from Figure 2 that creates tension in extensional flow is likely to create streamline tension in shear.

BOGER FLUID DESIGN & DECOUPLED RHEOLOGY

Boger fluids are specially designed to exhibit shear normal stresses and extensional thickening, but negligible shear thinning (James 2009). They are useful for scientific studies to isolate and understand elastic streamline tension effects separately from shear thinning, and are reasonably modeled with the Oldroyd-B constitutive equation, which has no nonlinear parameter (thus inherently linking linear viscoelastic parameters to the nonlinear effects). From a microstructure design perspective, Boger Fluids are achieved by cleverly starting with a high viscosity solvent and adding a dilute polymer (Figure 1); the polymer adds little to the shear viscosity, so its stretch and orientation have minimal shear thinning effect, but large streamline tension occurs in both shear and extension. Such decoupling of functionality is often desired in design methods (Ulrich et al. 2020). The ability to independently control decoupled rheological properties has not been systematically explored, though something similar to a Boger fluid has been achieved for yield-stress fluids with variable extensibility but negligible change in shear flow properties (Rauzan et al. 2018).

3.2. Shear Normal Stress Difference

A positive normal stress difference coefficient $\Psi_1 \equiv N_1/\dot{\gamma}^2 > 0$ is most often caused by positive streamline tension, which is primarily responsible for the rod climbing in Figure 1 (Beavers &

Joseph 1975). The flow is complex but predominantly shear, with azimuthal velocity decreasing away from the rotating rod. Inertial effects would tend to lower the free surface near the center, but tension along curved streamlines creates a hoop stress that increases the net force inward. If large enough to counteract inertial effects, it drives the fluid up the rod as gravitational pressures grow to balance the hoop stress. To design for maximum rod climbing, one may decide to neglect the subdominant effects (such as the second normal stress difference Ψ_2) and simply maximize Ψ_1. This is readily achieved with sufficiently high molecular weight polymers. In Figure 1 the blue aqueous solution has 2wt% poly(ethylene oxide) (PEO) with average molecular weight $M_w \approx 8{\cdot}10^6$ g/mol.

Shear normal stress N_1 is useful in thrust bearings (Sharma & Yadav 2014), journal bearings (Nessil et al. 2013), extrudate swell (also known as die swell) (Baird & Collias 2014), and particle focusing in microfluidics (D'Avino et al. 2012, 2017; Kim et al. 2019; Leshansky et al. 2007; Yang et al. 2011). The sub-dominant N_2 can also be important, e.g. if it is negative it can help provide a recentering force in wire coating (Tadmor & Bird 1974), but in many cases maximizing or minimizing N_1 is the design criteria.

The typically undesirable extrudate swell effect (Figure 4d) from a straight channel is thought to be primarily caused by N_1 and the associated recoverable elastic strain; at the exit the remnant elastic tension along streamlines, due to the shear of the no slip wall, recoils axially to expand the diameter. A useful estimate for the ratio of diameter increase due to this effect is $D/d = \left[1+\frac{1}{2}\left(N_1/2\sigma\right)_w^2\right]^{1/6}$ where the subscript w indicates evaluation at the wall in the fully developed confined flow (Tanner 1970, 2005). This expression is useful for design, since it identifies the conceptual cause, N_1, and the result is material agnostic, written in terms of measurable viscometric functions applicable to any complex fluid, not just polymer melts. To

minimize extrudate swell below a critical value, one must minimize the ratio of normal to shear stress, either by decreasing the flow or reformulating the fluid. Extrudate swell can be more complex (Baird & Collias 2014), and result in predictive relations that are not as friendly for design, including expressions devoid of N_1 and instead written in terms of the linear viscoelastic relaxation time τ, even though linear viscoelasticity is not enough to cause the effect. Take caution! Connecting the nonlinear N_1 to the linear τ is common but material dependent: it primarily applies only for basic polymeric materials, but not microstructures that break down in flow, such as the flocculated colloidal suspensions extruded in some 3D printing applications.

Particle focusing in microchannels (Figure 3, Figure 4c) is also accomplished by shear normal stresses, as demonstrated experimentally by (Leshansky et al. 2007) and reviewed recently by (D'Avino et al. 2017). Here we consider the rheological design criteria. First derived by (Ho & Leal 1976) for a second-order fluid, both $N_1 > 0$ and $N_2 < 0$ can cause migration of particles to the center of Poiseuille flow. N_1 is typically much larger than N_2 for polymeric fluids; focusing on N_1, the physical rationale is that tension along curved streamlines acts around a particle, and there is higher tension at higher shear rates, causing a net force toward the lower shear rates at the center of the channel. This scales as $F_y \sim -a^3\left(\partial N_1(\dot{\gamma})/\partial y\right)$ where a is the particle radius. (Leshansky et al. 2007) extended the scaling law to estimate the expected particle velocity. Assuming F_y is counter balanced by Stokes drag, $F_\eta = 6\pi\eta(\dot{\gamma})Va$, the velocity scales as $V \sim \frac{a^2}{6\pi\eta(\dot{\gamma})}\frac{\partial N_1}{\partial \dot{\gamma}}\frac{\partial \dot{\gamma}}{\partial y}$. This is an excellent equation for design. It is microstructure agnostic: N_1 could come from any of the microstructures of Figure 2. It also shows the sensitivity to changing parameters. Larger particles should move faster, all else being equal. A dilute additive should deviate from Newtonian by first introducing a normal stress difference N_1, e.g. dilute polymers could be added to cause particle focusing.

These scaling laws can be used to derive a rheological design criterion. In the dilute limit where a second-order fluid applies, N_1 is related to τ as $N_1 = 2\eta\tau\dot{\gamma}^2$, and we can use this with the above equations to estimate a minimum τ for meaningful particle migration within a finite channel length L. Assuming parabolic flow in a tube of radius R with volumetric flowrate Q, and that particles must travel radially a characteristic distance R toward the center during the transit time $t = L/\overline{V}$ with $\overline{V} = Q/\left(\pi R^2\right)$, then the rheological design criteria for sufficient relaxation time is estimated by

$$\tau > \tfrac{3\pi^2}{32} R^6 / \left(a^2 Q L\right) \tag{2}$$

for particle focusing due to N_1. Note the extreme sensitivity to R, the lack of viscosity in the final expression, and the interesting result that faster flow promotes focusing even though this shortens the transit time. This design guideline helps explain why colloidal nanoparticles (not just polymers) can be used, as in (Kim et al. 2019). For their flow conditions (R = 12.5 μm, Q = 20 μL/hr, L = 10 cm, a = 3 μm) the criterion suggests $\tau > 0.7$ μs is required. Their 16.2 nm diameter colloidal particles, which have a diffusion-based relaxation time of τ = 2 μs, will therefore satisfy the rheological design requirement of Eq. (2). However, as with any design criteria, caveats exist. The velocity scaling theory on which the criterion is based lacks a precise numerical prefactor. An equation similar to Eq. (2) can be derived by inverting the design rule for channel length L given in (D'Avino et al. 2012) to solve for relaxation time; those authors consider a more specific condition for focusing within a certain percentage of the channel cross section. Furthermore, real fluids with higher polymer or colloid concentrations will not be well-approximated as second-order fluids. Additional more complex effects will exist beyond the scaling law: particle inertia and shear-thinning can cause some particles to migrate to the wall, and shear-thinning seems to have an additional effect of making focused particles regularly spaced

along the centerline (Del Giudice et al. 2018). These are important effects with realistic formulations and non-dilute concentrations.

With few exceptions (see sidebar titled Boger Fluid Design & Decoupled Rheology), normal stress is accompanied by shear thinning, and increasing the N_1 effect increases the overall viscosity, which may be undesirable. This tradeoff has been considered from a design perspective with hydraulic thrust bearings (Figure 4b) by (Lee et al. 2019), results shown in Figure 6. That work applied realistic model selection, surrogate modeling, and multi-objective design methods to consider co-design of both the fluid rheology and the thrust bearing surface topography. From the microstructure-specific paradigm of fluids with polymer additives, the Giesekus model (Bird et al. 1987) was parameterized by two relaxation modes each having a timescale, added viscosity, and a nonlinear anisotropic drag parameter to optimize. The Pareto-set family of optimal solutions included fluid designs with both high- and low-loading of viscoelastic additive, coupled with different surface texture shapes, summarized in Figure 6. This work shows how surrogate modeling can manage computational costs, and how multi-objective optimization tools can navigate realistic complex fluid design tradeoffs.

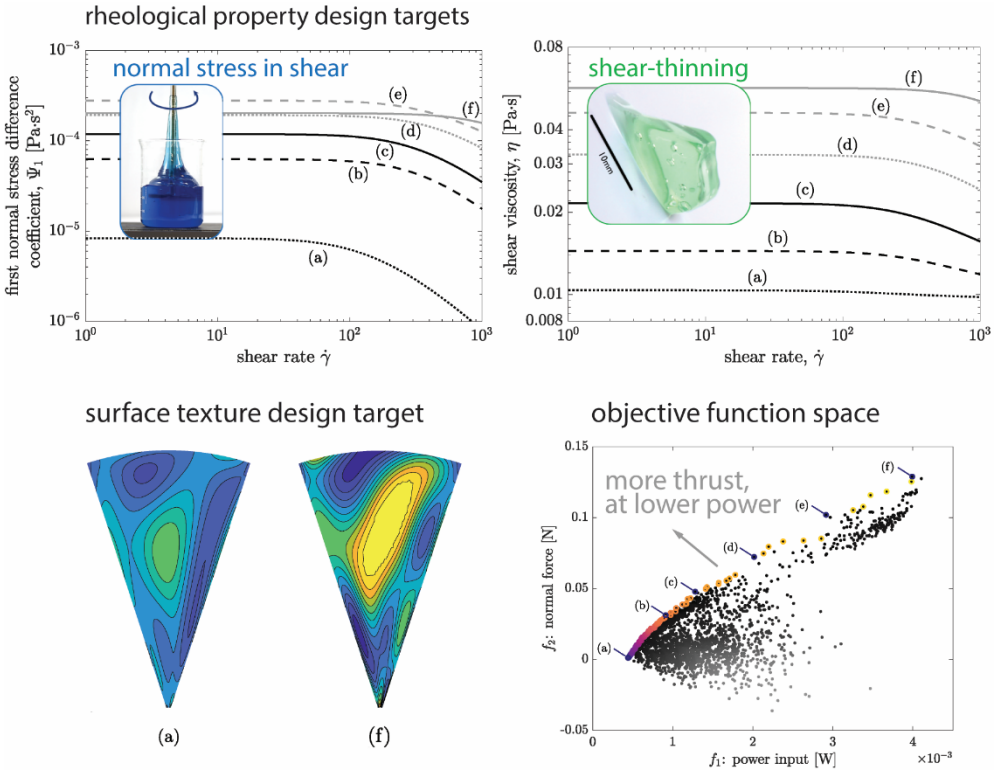

Figure 6: Design trade off with normal stress Ψ_1 and shear viscosity η for a multi-objective design objective: a hydraulic thrust bearing (Figure 4b) seeking to maximize thrust and minimize power input via co-design of polymeric solution properties and surface topography. These rheological functions are often coupled, as in this case where larger Ψ_1 comes at the cost of a larger η. Figures adapted from (Lee et al. 2019).

Shear normal stress and extensional thickening. In more complex flows (Figure 3), it can be difficult to determine if N_1 or extensional thickening $\eta_E > 3\eta$ is primarily responsible, since both phenomena involve streamline tension and are often simultaneously present in complex fluids (see sidebar titled Which Complexity Comes First?).

Streamline tension is beneficial in complex flows when it can reduce turbulent drag (Graham 2014; Lumley 1969; Virk 1975; White & Mungal 2008), or excite elastic instabilities / elastic turbulence (Steinberg 2021). Turbulent drag reduction, due to altered rheology, has found practical use in reducing pumping energy for the Alaskan oil pipeline (Burger et al. 1982) and enhancing hydraulic fracturing (King 2012). Minimizing turbulence by rheological design has

been suggested as a strategy to stop or "top kill" deepwater oil blowouts (Beiersdorfer et al. 2011). Elastic instabilities and turbulence can enhance mixing and heat transfer (Abed et al. 2016), improve oil recovery at lower than expected capillary number (Clarke et al. 2015), create emulsions (Poole et al. 2012), and make microfluidic flow diodes (Groisman & Quake 2004). Below we outline the rheological design perspective for flow diodes and turbulent drag reduction.

Microfluidic fluid diodes (Groisman & Quake 2004) have asymmetric flow resistance attributed to elastic instabilities caused by streamline tension. However, their complex flow makes design and optimization difficult. Optimization questions have been applied to the geometry (Jensen et al. 2012b,a), but not the fluid rheology. Modified geometries have experimentally achieved diode ratios above a factor of six (Sousa et al. 2012). The key dimensionless groups seem to be *Wi* and the Elasticity number, *El*. These are both typically written in terms of the linear viscoelastic relaxation time τ, but this is a surrogate for the nonlinear streamline tension. We discussed this issue in Section 2.2 for *Wi*, which can be written as either $Wi = \tau\dot{\gamma}$ or $Wi = N_1/2\sigma = \frac{\Psi_1}{2\eta}\dot{\gamma}$. The Elasticity number (Astarita & Marrucci 1974) is most fundamentally defined as the ratio of normal stress to inertia, but commonly written in terms of linear viscoelastic relaxation time as a surrogate for normal stress as $El \equiv \tau\eta/(\rho l^2)$, where η is solution viscosity, ρ fluid density, and the characteristic lengthscale of the device is *l* (Rodd et al. 2005, 2007). It is more direct to define as $El \equiv N_1/\rho V^2 = \Psi_1/\left(\rho l^2\right)$, where the final expression makes use of the definition $\Psi_1 \equiv N_1/\dot{\gamma}^2$ and takes characteristic strain rate $\dot{\gamma} \sim V/l$. This reveals the importance of elastic normal stresses, and recovers the form $El = 2\tau\eta/(\rho l^2)$ only if $\Psi_1 = 2\eta\tau$ (as with the second-order fluid and some polymer-based models). The relation between τ and Ψ_1 is both good and bad for design. It is good when the surrogate relation works, as the complex fluid design can

shift focus from Ψ_1 to τ, where much is known (see Section 4.2). It is bad if $\Psi_1 = 2\eta\tau$ is insufficiently accurate. For example, a flocculated colloidal gel can become solid, having an incredibly large relaxation time τ, but this does not translate to a large *El* because under flow, aggregates break, and do not stretch, so there is little if any streamline tension N_1.

Turbulent drag can be substantially reduced by the addition of small amounts of polymer to the flow (Lumley 1969; Virk 1975; White & Mungal 2008), although the physics of this is not well understood (Graham 2014). The effect has been attributed to the stretching of polymers in the flow, but a range of other additives also produce the effect, including surfactants, platelets, and fibers (Lee et al. 1974; Paschkewitz et al. 2005). Both "viscous" (Lumley 1969) and "elastic" (Tabor & De Gennes 1986) classes of explanations exist (White & Mungal 2008), though both can be associated with extra tensile stress along streamlines and an increase in extensional viscosity. From the rheological design perspective, insight was produced by (Roy et al. 2006) who considered a microstructure-independent model (the ordered fluid expansion up to fourth order) and how it affects turbulence near its onset. They conclude that the biaxial extensional viscosity of the fluid, a measurable property agnostic to microstructure, affects the turbulent structures resulting in drag reduction. Higher-order effects are, of course, more complicated. The most extreme condition is the observation of an apparent "maximum drag reduction" asymptote (Virk et al. 1970), which has been rationalized with polymer-based models (Xi & Graham 2012), but with recent claims of being exceeded with polymeric additives (Choueiri et al. 2018). A key design tradeoff is that increasing the polymer molecular weight can enhance the effect, but higher molecular weight polymers are also more susceptible to degradation and clogging of pumps. Alternatives based on associated polymers seem to provide a separate design route to achieving required nonlinear elastic properties (Wei et al. 2015a).

3.3. Extensional Thickening

When flow is primarily extensional, the key property to design is the extensional viscosity η_E, which can be large compared to the Newtonian expectation of $\eta_E = 3\eta$. The polymeric liquids of Figure 2 create especially large ratios of η_E/η, but other microstructures also lead to large extensional viscosity. In Figure 1, the self-emptying open siphon is stabilized by resistance to elongational flow; this is a key aspect of many useful applications.

Extensional thickening enables flow objectives ranging from molecular gastronomy to manufacturing. Traditionally, it has been used in polymer processing to enable very thin filaments and films (fiber spinning, film blowing, foaming) (Münstedt 2018), and this continues to be important in the development of new polymers including sustainable bioplastics. Many other flow objectives can be achieved. Extensional thickening can reduce fire risk via anti-misting jet fuels (Wei et al. 2015a), reduce misting in roll coating (Owens et al. 2011), eliminate satellite droplets in inkjet printing (Wijshoff 2010), suppress droplet rebound in agricultural sprays (Bergeron et al. 2000), improve rising of bread dough (Dobraszczyk & Morgenstern 2003), increase strength of adhesives in tension (Verdier & Piau 2003), enable bubble blowing with chewing gum (Martinetti et al. 2014), enable the performance magic of Mystic Smoke (Nelson 2018), and make giant soap bubbles (Frazier et al. 2020).

Many cases require a large elongational viscosity η_E to meet objectives, but the design criteria can also be nuanced (or unknown) depending on the application. A microstructure-agnostic criteria for filament breakup due to necking instability, known as the Considère condition (Considere 1885), has been applied to viscoelastic fluids in high rates of extension (McKinley & Hassager 1999). The condition for stability is that tensile force does not decrease with strain, e.g. in uniaxial extension $dF_z/d\varepsilon \geq 0$. This translates to $d\ln T_{zz}/d\varepsilon > 1$ where ε is the true strain and

$T_{zz} = \sigma_{zz} - \sigma_{xx}$ is the total traction stress on the ends. The Considère condition is simple and useful, being applied to materials as complex as bread dough (Dobraszczyk & Morgenstern 2003; van Vliet 2008), but it has been found lacking for some polymer melts (Barroso et al. 2010; Joshi & Denn 2004). Other criteria have been suggested, such as a critical recoverable strain in extension (Joshi & Denn 2004). Recently, necking criteria have been refined to include additional mechanisms which better predict failure across several nonlinear viscoelastic constitutive models (Fielding 2011; Hoyle & Fielding 2016). The criteria are expressed in a material-agnostic fashion, related to the continuum-level stress versus strain (or time) response. Microstructure-specific reasons can also be surmised for failure in extension, e.g. as done for polymer melts (Zhu & Wang 2013).

Extensional viscosities can also be too large for some goals, which makes a maximum extensional viscosity the design condition. In dispensing applications, including inkjet and direct-write printing, filament breakup is required and typically driven by surface tension Γ. Here, long filament-breakup times may be problematic, resulting in stringy or messy deposition, with the resulting breakup inhibited by extensional viscosity or inertia. Since extensional viscosity has complex dependence on the strain rate, at least three independent dimensionless groups are needed to construct the so-called "map of misery" operating space: Weber (*We)*, Capillary (*Ca*), and Weissenberg (*Wi*) (Clasen et al. 2012), as shown in Figure 7. Other relevant dimensionless groups can be constructed from these, including the important Ohnesorge number (*Oh*), which can be interpreted as the ratio of inertio-capillary to visco-capillary velocities,

$$Oh = \frac{U_{inertio-cap}}{U_{visco-cap}} = \frac{\sqrt{\Gamma/(\rho R)}}{(\Gamma/\eta)} = \frac{\eta}{\sqrt{\rho \Gamma R}}. \quad (3).$$

This can estimate which of the two velocities is slower and therefore which effect (inertia or viscosity) dominates the time required for pinch-off. All these dimensionless groups act as microstructure-agnostic design criteria for rheological properties, but again caution is required as the extensional thickening suggested by Wi is often mapped to a linear viscoelastic timescale τ based on assumptions from polymeric liquids, and this may not apply across all material microstructures (Figure 2). To fully embrace the nonlinearity, there are practical index tests, including tensile tests of melt strength (The International Organization for Standardization 2021) and uniaxial extension rupture length (Frazier et al. 2020; Rauzan et al. 2018), which can serve as design targets, though these extensive properties may obfuscate the design insight offered by intensive rheological functions.

Material-agnostic criteria give a design guideline for what properties are needed, abstracted away from molecular details, providing a more universal perspective and a design target that might be achieved by multiple microstructural mechanisms. How many molecular and microstructural mechanisms are possible to increase (or decrease) extensional viscosity and inhibit failure? Possible microstructure design strategies include rod-like particle additives, high molecular weight polymers that can be linear or branched, lower molecular weight polymers with transient crosslinks (some of which may exchange intra- to inter-molecular crosslinks for increased thickening), wormlike micelles which may undergo a phase transition (Vasudevan et al. 2010), megasupramolecular associating polymers (Wei et al. 2015a), flow-induced crystallization (Wingstrand et al. 2018), molecular elongation combined with solvent evaporation as with spider silk (Kojic et al. 2006), and likely other mechanisms to cause the tensile stress to grow sufficiently fast with extensional deformation.

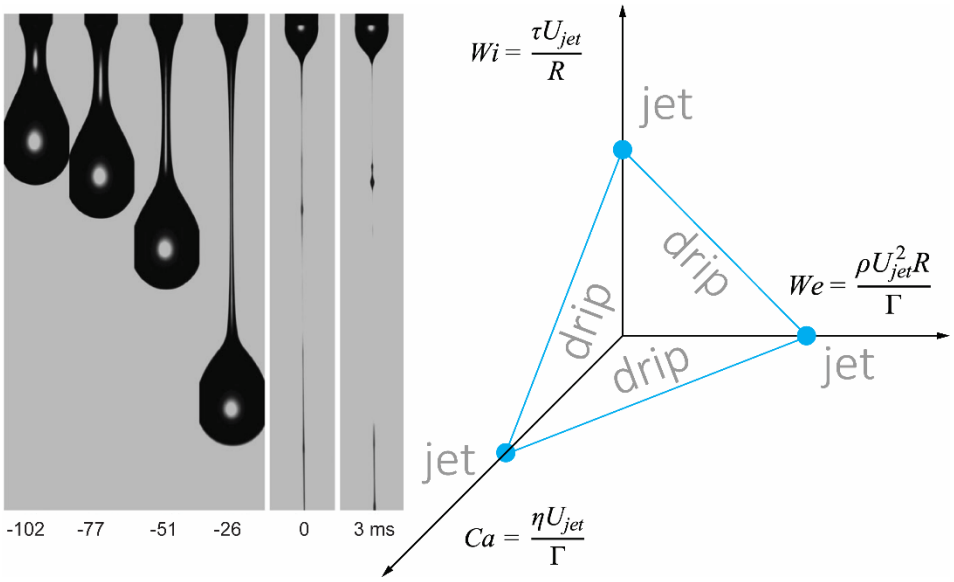

Figure 7: The "map of misery" for "drip" versus "jet" behavior of an extruded fluid. Left image shows a single example of a drip condition, defined by occurrence of pinch-off (at 0 ms). Faster velocity U_{jet} would transition this to jet behavior that avoids pinch-off. The regime map with Weissenberg number Wi on the vertical axis is an example of using the linear relaxation time τ as a surrogate for the nonlinear effects of extensional viscosity η_E. Figure adapted with permission from (Clasen et al. 2012).

3.4. Nonlinear Viscous

Shear thinning and shear thickening are complementary ways to be non-Newtonian, with shear viscosity a function of the forcing stress or strain rate. Shear thinning is a broad category of behavior and includes, as a subset, yield-stress fluid behavior with a solid-like high viscosity at low stress (as in Figure 1), and as a corollary, thixotropic time-dependence of shear thinning, which can be an important design consideration when rapid recovery of the viscosity, modulus, or yield stress is exploited to hold a fluid in position. The terminology of thixotropy and shear thinning are often confused in patents and papers, and this unfortunately obfuscates design insight. Shear thinning is the flow strength dependence of the shear viscosity, whereas thixotropy relates to its time dependence, which is realized with the time-dependent breakdown and recovery of

microstructure. This distinguishes it from viscoelastic time dependence (Mewis & Wagner 2009). Yield-stress fluid design has been recently treated in detail in a focused review (Nelson et al. 2019) and paper (Nelson & Ewoldt 2017). Here we look more broadly across the landscape of useful nonlinear viscous rheology.

Shear thickening. Shear thickening is a subject of active scientific inquiry (Morris 2020) and is a visually striking way to show unexpected non-Newtonian behavior, e.g. by walking on a pool of shear thickening liquid (typically corn starch particles at high volume fraction in water (Niu et al. 2020)). Shear thickening has far fewer applications than shear thinning, but a notable use is high flow rate energy dissipation by introducing shear-thickening fluid into fabrics, including ballistic vests (Wagner & Wetzel 2010), athletic tape (Holt & Perez 2015), and sports bras that claim to restrict movement when the shear stress exceeds a threshold value (Witek et al. 2020). In each case, key design criteria include the amount of thickening required (so-called discontinuous shear thickening is much more extreme than continuous shear thickening), and the nominal critical stress σ_{crit} at which the thickening occurs. Current thinking seems to focus on critical stress rather than critical strain rate, including in patent claims (Witek et al. 2020), which may clarify design targets since stress is often known independent of the rheology in applications (Corman & Ewoldt 2019).

How many ways are there to make a shear thickening fluid? The predominant approach is to use particles at sufficiently high volume fraction (as in the cornstarch particles in water demonstrations), but transient polymer networks such as poly(vinyl alcohol)-Borax (Martinetti et al. 2018) and shear-induced attractive colloid gelation are also possible.

Shear thinning without yield stress. Many additives are available to increase viscosity and create shear thinning (Ash & Ash 2006; Braun & Rosen 2000), and this can be useful even without creating a yield stress. Familiar examples include thickened culinary sauces to improve mouthfeel and artistic plating with swirls and pushes (Mouritsen & Styrbæk 2017). For people with swallowing difficulty, known as dysphagia, products are available to thicken liquids with the intention of slowing the flow under gravity but with easy flow under applied additional stress during swallowing; shear thinning is of primary importance, though recent studies suggest elastic extensional viscosity may also be desired (Nyström et al. 2015). Wildland fire suppression can also employ aqueous shear thinning fluids (US Forest Service 2020), though rheological design targets are less clear and yield-stress fluid behavior seems beneficial for this complex scenario. Further familiar applications include paint, shampoo, and cosmetics (Spicer et al. 2020).

Quantitative design targets include the critical stress for thinning, the sensitivity (often power law) of stress to strain rate, or the amount of shear thinning. Most reported quantitative insight comes via the simplifying assumption of a power law fluid with shear stress response $\sigma = m\dot{\gamma}^n$, and then considering design regarding m and n. A recent example involves injectable hydrogels (Lopez Hernandez et al. 2020) where the maximum force required for a person to press a syringe plunger ($F < 50$ N) is a design criterion. By inverting the fluid mechanics equations for power-law flow in a pipe, the authors craft a design criteria for the power-law parameters, using a clever Ashby-style coplot of consistency index m and shear-thinning parameter n, and limit lines that depend on needle dimensions.

Nearly every microstructure shows some type of shear thinning and this is perhaps the most common type of rheological modifier in the handbooks. For design intuition, there are three main

microstructural routes to significant shear thinning: alignment in the flow direction, breakdown of structure, and friction/sliding in high volume fraction systems.

Yield-stress fluids: extreme shear thinning. The most useful shear thinning is often the most extreme: an effectively solid-to-liquid reversible transition at a critical stress (or range of stress). Uses of this viscoelastic solid-like to fluid-like transition are wide ranging (Nelson et al. 2019). Noteworthy applications include direct-write 3D printing (Truby & Lewis 2016), bioprinting with suspended live cells having higher viability in the plug flow region (Olsen et al. 2010; Yan et al. 2012), injectable hydrogels for release of therapeutic agents (Li & Mooney 2016), embedded 3D printing (Nelson et al. 2020b; O'Bryan et al. 2017), flow battery working fluids (Wei et al. 2015b), foods and personal care products for texture perception and stabilizing suspended particles, magnetorheological fluids for smart prosthetics (Carlson et al. 2001), wildland fire suppression coatings (Hagquist et al.; Yu et al. 2019), and wall-climbing robots (Ewoldt et al. 2007); several of these are shown in Figure 4.

Design criteria primarily involve the yield stress σ_y, starting with a minimum σ_y to retain solid-like behavior against gravity or surface tension effects. To suspend a particle of characteristic diameter D in a fluid, the criterion takes the form

$$\sigma_y > Y_g^* \Delta\rho g D \tag{4}$$

where Y_g^* is a dimensionless constant known as the critical yield-gravity parameter for onset of motion. For spheres, the theoretical value is $Y_g^* = 0.048$ (Beris et al. 1985), though some experimental values have been slightly larger, e.g. $Y_g^* = 0.088$ (Jossic & Magnin 2001). Similar minimum σ_y occur for other scenarios, such as maintaining a fluid coating of thickness h on a surface inclined at angle θ,

$$\sigma_y > \rho g h \sin\theta \tag{5}$$

or a wall-climbing robot using adhesive locomotion,

$$\sigma_y > W \sin\theta \Big/ \left(A\left(1-2\phi\right)\right) \tag{6}$$

with robot weight W, total contact area A, and areal fraction ϕ advancing forward (Ewoldt et al. 2007), or 3D printing that resists both gravitational and surface tension effects,

$$\sigma_y > \rho g h + \gamma R^{-1} \tag{7}$$

with maximum printing height h and filament radius of curvature R (M'barki et al. 2017). More complex criteria exist with multi-objective design, such as flow batteries which target high energy density, fast charge transport, and low-dissipation flow (Wei et al. 2015b).

The detailed shape of the stress versus shear rate curve does not seem to have been considered from an optimal design perspective, but low-dimensional metrics of this curve have been used for material selection, e.g. with Ashby-style diagrams for selecting a fluid for adhesive locomotion (Ewoldt et al. 2007), and for dimensionless groups to guide rheological design in droplet impact and splashing (Blackwell et al. 2015; Sen et al. 2020), motivated by fire suppression. Parameters for Ashby plots should have consistent dimensions, which motivated re-writing of the standard Herschel-Bulkley model for shear stress $\sigma = \sigma_y + K\dot{\gamma}^n$ as $\sigma = \sigma_y \left(1 + \left(\dot{\gamma}/\dot{\gamma}_{crit}\right)^n\right)$ where the model parameter $\dot{\gamma}_{crit} = \left(\sigma_y / K\right)^{1/n}$ has consistent dimensions (unlike K) of inverse time and a clear interpretation as the shear rate where viscous rate-dependent effects are comparable to the plastic yield stress σ_y (Nelson & Ewoldt 2017). Beyond the flow curve description of $\sigma(\dot{\gamma})$, yield-stress fluids have elasticity below yield and the elastic modulus G can be important for holding shape in 3D printing. Thixotropic restructuring of the yield stress must also be considered, as with the

hysteretic nature of the yield stress to start versus stop a flow, referred to as the static versus dynamic yield stress, respectively.

More recently, extensional properties of yield stress fluids have been shown to be important (Nelson et al. 2018); high extensibility can be desirable, as in 3D printing (Rauzan et al. 2018), or undesirable, as in sprayability (Lin et al. 2020). At present, the observed extensibility with yield-stress fluids is not adequately captured by predictive constitutive models for $\underline{\underline{\sigma}}$ in Eq. (1). Design progress has thus been driven by conceptual models, rather than mathematical models, with much consideration at the microstructural level. Operating maps similar to the "map of misery" (Figure 7) might be expected to describe the bounds for filament breakup with elastic yield stress fluids. Unlike in Figure 7, the linear viscoelastic timescale τ likely cannot serve as a surrogate for expected nonlinear extensional viscous effects, and new dimensionless groups will be required.

From a microstructure perspective, a yield-stress fluid is created with a sample spanning network using two possible strategies: attractive or repulsive interactions (Nelson & Ewoldt 2017). These categories are sometimes referred to as "gel" versus "glass"; representative examples in Figure 2 are the flocculated colloids forming a percolated network and the jammed soft particle suspension. For a list of possible materials to use in practice, see Table 1 and Fig.6 in (Nelson et al. 2019). Most microstructures have scaling laws to understand and predict the sensitivity of σ_y, as summarized in Table 1 of (Nelson & Ewoldt 2017).

Thixotropic time dependence of shear thinning. The time-dependent recovery of viscosity, elastic modulus, and yield stress is typically sought to be fast. For example, to maintain shape after extrusion-based printing, fast recovery after deposition is needed. Design criteria would then typically appear as $\tau_{thixo} < \mathcal{T}$ where $\mathcal{T}$ depends on the problem to be solved, e.g. the time for

gravitational sag to be significant in the 3D printing example, or the time to take a subsequent step with the robotic adhesive locomotion. In this way, the thixotropic recovery time is a nuisance to be minimized.

A noteworthy case of useful thixotropy is for self-smoothing paints and coatings. After application forces are removed, before thixotropic recovery is complete, surface tension or gravity can act to smooth, flatten, and/or level the surface, followed by full thixotropic recovery to keep the coating in place. This would suggest a design criteria in the form $\mathcal{T}_1 < \tau_{thixo} < \mathcal{T}_2$, where the mechanisms of self-smoothing sets $\mathcal{T}_1$ and longer time effects such as gravitational sag set $\mathcal{T}_2$. Similar concepts may apply to three-dimensional cell culture using thixotropic materials, where the stirred liquified state allows cells to be added, followed by thixotropy recovery of the solid-like properties (Pek et al. 2008).

The design freedom for thixotropy may not be τ_{thixo} directly, but the underlying dynamics of structure destruction and aggregation, e.g. as typified by the empirical Moore model (Moore 1959) for dimensionless structure parameter ξ, given as $d\xi/dt = -k_d\dot{\gamma}\xi + k_a(1-\xi)$. Using adjoint-based sensitivity methods, (Freund et al. 2018) posed the design-inspired question: how sensitive is a quantity of interest (drag on a sphere) to the parameters k_d and k_a at each location in the flow field? Figure 8 gives the answer for a particular flow strength. Note how the sensitivity to k_d occurs upstream (below), and the sensitivity to k_a occurs downstream but also upstream, in a contiguous region around the sphere. From a fluid design perspective, if properties in a particular region of flow can enhance behavior, then local control (such as local heating with a laser), rather than global control, may be a strategy for achieving flow objectives.

Whether minimizing or targeting thixotropic dynamics, thixotropic recovery times tend to be longer for sparse attraction-based systems compared to crowded systems (Ewoldt et al. 2007).

Clever use of shear banding also seems to enable rapid recovery, as observed with injectable hydrogels from telechelic proteins (Olsen et al. 2010). Establishing scaling laws for thixotropic timescales, across a range of possible microstructures, remains a goal.

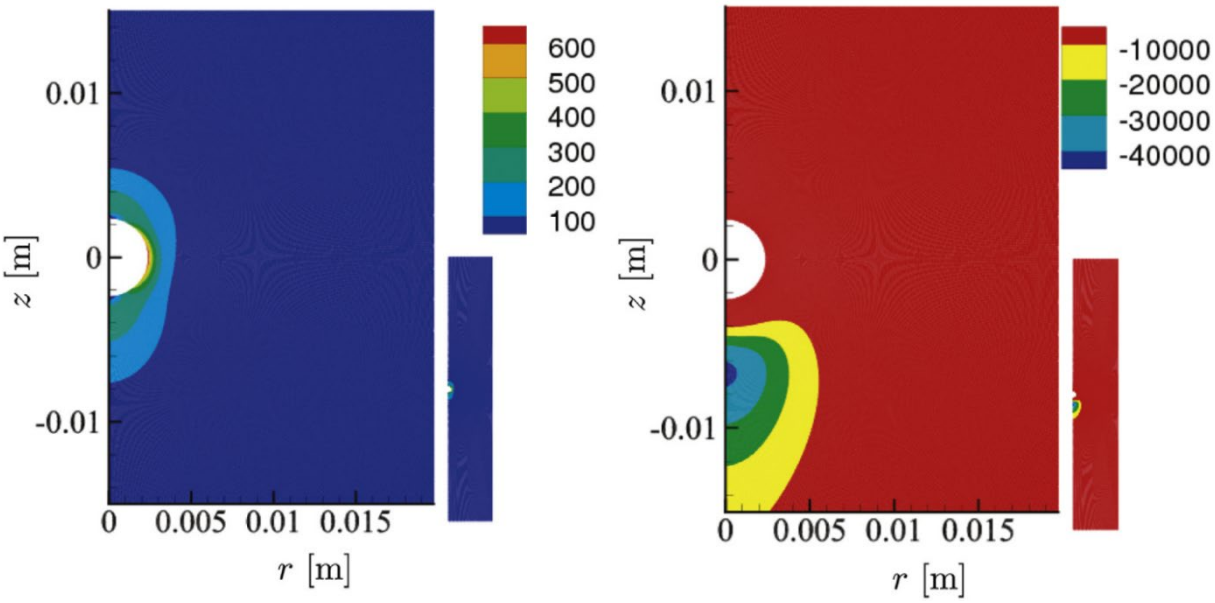

Figure 8: Field sensitivity of flow predictions to shear-thinning thixotropic model parameters for a sphere (white half circle in axisymmetric space); color maps show quantitative sensitivity of drag force to (a) aggregation (build up) constant k_a, and (b) destruction (breakdown) constant k_d. Figure used with permission from (Freund et al. 2018).

3.5. Beyond the Key Phenomena

For many fluids, all the key rheological phenomena are present, and multiple may be important in combination for achieving the objectives. Terms like "Thixo-elasto-visco-plastic" (TEVP) (Ewoldt & McKinley 2017) hint at all aspects of the rheological phenomena described here. But

there is even more complexity beyond the realm of intensive rheological material functions. These include shear banding, fracture, wall slip, and confinement effects, which may be important and even useful for applications, as especially noted in tribology-related settings (Stokes et al. 2013).

4. DESIGN TOOLS: A FLUID MECHANICS PERSPECTIVE

Design methods are often based on analysis and scientific understanding, but re-framed to facilitate answers to the inverse-problem questions posed in Section 1. Several design tools emerge in the survey of Section 3. These include design-driven model selection, low-dimensional descriptions of rheological properties, dimensionless groups, scaling laws that relate rheological properties to flow objectives, scaling laws that relate microstructure to rheology, material-agnostic constitutive modeling, sensitivity analysis, and optimization methods. Many of these are standard approaches in fluid mechanics that, if properly framed, become design friendly. Design tools apply to the range of rheological phenomena. Two aspects deserve a more integrated discussion: model selection at the continuum-level, and comparative scaling laws at the microstructural level.

4.1. Model Selection for Design

There are countless models for non-Newtonian constitutive behavior of $\underline{\underline{\sigma}}$ in Eq. (1). How can this complexity be organized? How should a model be selected for fluid design? Where can flow and rheology be separated from microstructure and chemistry?

The Pipkin map (Pipkin 1972), as adapted in Figure 9, provides a framework for answering these questions. Newtonian behavior exists at the origin, and three different axes quantify deviation from Newtonian behavior: *De* for viscoelastic time dependence, *A* for nonlinear flow strength dependence (however it is best defined), and τ_{thixo}/t for thixotropic time dependence. The

isotropic Newtonian limit is material agnostic, since a single equation can be assumed to govern behavior, independent of the chemistry or microstructural details. Of course, the Newtonian viscosity depends on the chemistry, but it is abstracted into the property and design questions can be posed for identifying optimal viscosity, knowing that this is a universal description for all fluids in this limit. This is not the case in the interior regions of the Pipkin map, but along the edges similar universal equations helpfully exist. We have seen several play a role in Section 3.

For incompressible linear viscoelasticity, the Boltzmann superposition equation governs all behavior, as noted in Section 3.1. The associated continuous relaxation spectrum $H(\tau)$ is a design-friendly starting point to represent viscoelasticity. Optimal shapes of $H(\tau)$ can be sought and the design freedom constrained by the realities of available microstructural relaxation spectra (Corman 2019). This may also serve as a springboard for posing design optimization questions with the Memory Integral Expansion (Bird et al. 1987) for weakly nonlinear but fully viscoelastic flows.

The ordered-fluid expansion theoretically applies to all microstructures in slow and slowly varying flows, i.e. small *A* and *De*. We saw that a second-order fluid, which can be considered the smallest step away from Newtonian, includes three of the four key phenomena in Figure 1 (it cannot predict shear thinning), and provides useful insight for relating linear viscoelastic relaxation time τ to the onset of nonlinear effects Ψ_1 and η_E, and motivates use of τ as a surrogate for expectations of nonlinearity. A third-order fluid is needed for emergence of nonlinear viscous behavior (e.g. shear thinning), which has provided material-agnostic insight into turbulent drag reduction (Roy et al. 2006). The nonlinear viscous region is another limit with a universal equation, the Reiner-Rivlin fluid, $\underline{\underline{\sigma}} = \eta_1(II_{\dot{\gamma}}, III_{\dot{\gamma}})\underline{\underline{\dot{\gamma}}} + \eta_2(II_{\dot{\gamma}}, III_{\dot{\gamma}})\left(\underline{\underline{\dot{\gamma}}} \cdot \underline{\underline{\dot{\gamma}}}\right)$. Here the design freedom is the dependence of η_1 and η_2 on the second and third invariants of $\underline{\underline{\dot{\gamma}}}$. More commonly, a subset

of this expression is used, known as the generalized Newtonian fluid, $\underline{\underline{\sigma}} = \eta(\dot{\gamma})\underline{\underline{\dot{\gamma}}}$, where the design freedom is the shape of the measurable viscosity function $\eta(\dot{\gamma})$.

Beyond the borders, no universal descriptions are available. Choosing a constitutive model may be motivated by an assumed microstructure, e.g. polymer solutions (Larson & Desai 2015b), as with the Giesekus model in (Lee et al. 2019). (Fielding 2011) explored five different models of polymer rheology in search of more universal insight. It is noteworthy that popular models such as Oldroyd-B and corotational Maxwell have no nonlinear parameters, limiting their design freedom to linear viscoelastic properties, even if nonlinear behavior is relevant for the flow objective. Whether this is a benefit or detriment for design is an open question, as a model with fewer (and linear) parameters may be more tractable but misses possible behavior and decoupled design in real fluids. Thixotropy is less explored and less understood. As a whole, our current list of constitutive equations still cannot reproduce all experimental observations of rheological complexity in $\underline{\underline{\sigma}}$, even missing important phenomenology (see sidebar titled Don't Rely on Equations Alone).

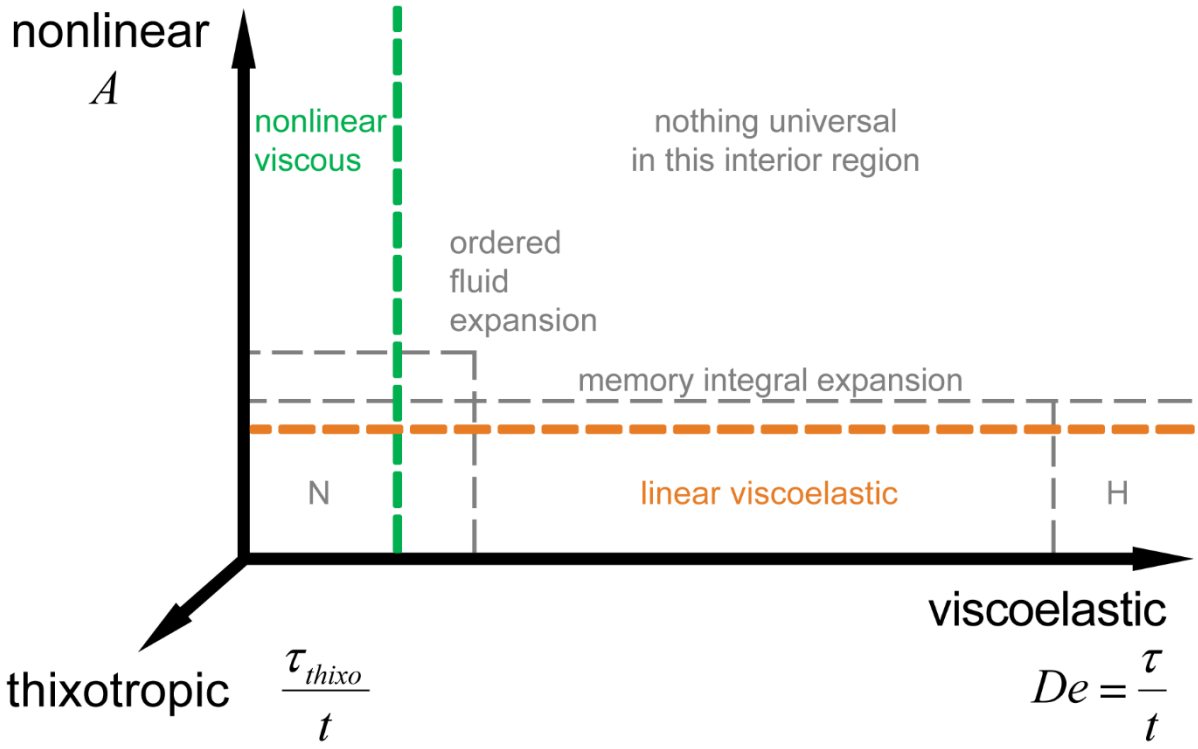

Figure 9: Universal design insight may be available near the edges of this Pipkin map, where constitutive behavior is material-agnostic and a master equation exists in the indicated regions. The nonlinear behavior axis is characterized by a dimensionless flow strength A, which can be expressed in terms of stress, strain rate, or strain. Boundaries are fuzzy, depending on the threshold for neglecting higher order effects. N: Newtonian viscous fluid, H: Hookean elastic solid, other regions as described in the text.

DON'T RELY ON EQUATIONS ALONE

New paradigms of phenomenology are possible beyond what can be currently predicted by constitutive models. For example, only recently was it shown that many shear-thinning yield-stress fluids can have high extensional viscosity (Nelson et al. 2018), and that this can be controlled to improve direct-write 3D printing performance (Rauzan et al. 2018). This was experimentally discovered and designed with conceptual models, rather than optimizing available mathematical models.

4.2. Scaling Theories for Rheology-to-Structures

As suggested by the Pipkin map of Figure 9 and the ordered fluid expansion, the linear viscoelastic relaxation time τ is a starting point to understand other rheological complexity. It is also the most well understood in terms of scaling laws across a range of different microstructures, which are summarized in Table 1. Even in the absence of numerical prefactors, design insight is supported by knowing sensitivities, especially to lengthscale L. The expressions in Table 1 are written to emphasize the parallel structure of the form $\tau \sim \eta/G$ and $\tau \sim L^{\alpha}$ where $\alpha = 3$ for many cases.

Similar collected comparisons for other key properties are being developed, as for the yield stress σ_y, Table 1 in (Nelson et al. 2019). High-fidelity computations of microstructure can also provide insight, especially where scaling laws are not yet available or insufficient to represent the complexity, including scenarios where non-homogeneous microstructure deformation is important for overall behavior, as in localized yielding in attractive colloidal gels (Colombo & Del Gado 2014). A noteworthy example that crosses the entire design hierarchy is the work of Read, McLeish, and co-workers to relate flow behavior of branched entangled polymer systems to the design freedom of the polymerization chemistry details (Read et al. 2011). For any simulation, consideration must be given to interfacing with wrapper functions to accelerate exploration and interface with surrogate modeling and optimization routines.

Table 1. Comparison of the many ways to change a linear viscoelastic relaxation time.

System	Mechanism	Scaling relations	Comments
Dilute polymer solution	Entropic spring (Rubinstein & Colby 2003)	$\tau \sim \frac{\zeta}{K} \sim \frac{\eta_s}{kT/R_g^3}$	Zimm model (Tirtaatmadja et al. 2006) $\tau = \frac{1}{\zeta(3\nu)} \frac{[\eta]\eta_s M_w}{N_A k_B T} \sim M_w^{3\nu} \sim R_g^3$
Spherical particle suspension	Translational diffusivity (Larson 1999)	$\tau \sim \frac{a^2}{D_t} \sim \frac{\eta_s}{kT/a^3}$	Stokes-Einstein $\tau = 6\pi\eta_s a^3 / kT$
Rod-like particle suspension	Rotational diffusivity (Larson 1999)	$\tau \sim D_r^{-1} \sim \frac{\eta_s}{kT/L^3}$	For high aspect ratio L/d: $D_r = 3kT\left(\ln(L/d) - 0.8\right)/\left(\pi\eta_s L^3\right)$
Entangled polymer melt	Reptation diffusivity (de Gennes 1971)	$\tau \sim \frac{\bar{L}^2}{D_c} \sim \frac{\zeta_c}{kT/M_w^3}$	Typically observed to be $\tau \sim M_w^{3.4}$ (Berry & Fox 1968)
Emulsion droplets	Surface tension (Derkach 2009; Larson 1999)	$\tau \sim \frac{\eta}{\gamma/R}$	Not set by Brownian motion; different sensitivity to length scale than others
Flocculated colloids	Attractive energy well (Larson 1999)	$\tau \sim \frac{\eta_s}{kT/a^3} \exp\left(\frac{W}{kT}\right)$	Can diverge with strong attraction
Transient polymer network	Crosslink timescale (Rubinstein & Colby 2003)	$\tau \sim \frac{1}{\omega_0} \exp\left(\frac{W}{kT}\right)$	Can diverge with strong attraction
Wormy micelle surfactant	Chain breakage and reptation (Larson 1999) (Cates & Candau 1990)	$\tau \sim \sqrt{\tau_{br}\tau_{rep}}$	$\tau_{br} = 1/k_{br}\bar{L}$ $\tau_{rep} = \bar{L}^2/D_c$

Legend: $a \equiv$ particle radius; $d \equiv$ cylinder diameter; $D_r, D_t \equiv$ rotational, translational, reputational diffusivity; $D_c \equiv$ curvilinear diffusion constant of the chain in its tube; $k \equiv$ Boltzmann constant; $k_{br} \equiv$ scission-kinetic-rate constant; $K \equiv$ spring constant in the bed-spring model; $\bar{L} \equiv$ average chain length; $N_A \equiv$ Avogadro's number; $R \equiv$ droplet radius; $R_g \equiv$ radius of gyration; $T \equiv$ system temperature; $W \equiv$ strength of attractive potential; $\gamma \equiv$ interfacial tension; $\zeta \equiv$ Stokes drag friction coefficients in the bead-spring model; $\zeta_c \equiv$ polymer-polymer friction; $\zeta(3\nu) \equiv$ zeta function of argument 3ν; $\eta \equiv$ continuous medium viscosity; $[\eta] \equiv$ intrinsic viscosity; $\eta_s \equiv$ solvent viscosity; $\nu \equiv$ exponent characterizing the scaling of the equilibrium of R_g and M_w; $\tau_{br} \equiv$ breakage time; $\tau_{rep} \equiv$ reptation time; $\omega_0 \equiv$ natural frequency of thermal vibrations

5. CONCLUSION

The four key phenomena of Figure 1 organize how non-Newtonian design freedom can achieve diverse flow objectives. There are systematic approaches from fluid mechanics and design that

help connect from flow, to properties, to microstructural building blocks. Rheological property targets may be expressed as minimum or maximum targets, but also as targeted shapes of material functions, which themselves may comprise families of Pareto-optimal solutions. The inverse problem of engineering design is built upon the forward problem of analysis and scientific knowledge. There is opportunity to generate knowledge within this design paradigm, and mathematical challenges arise when trying to pose these inverse problems to identify complex properties and the possible molecules and structures which can provide them.

SUMMARY POINTS

1. Every rheological phenomenon has found creative and useful applications. This survey lays a foundation for uses not yet imagined.
2. Organizing principles for complex fluid design include the four key phenomena, dimensionless numbers, model selection, and the inverse rheology-to-structures perspective: many material structures are available to produce a desired rheological response.
3. Conflict between design freedom and realism must be considered on a sliding scale from completely free shapes of material functions to known shapes associated with pre-selected formulation options.
4. Linear viscoelastic relaxation time τ is often a surrogate for nonlinear shear normal stress Ψ_1 and extensional viscosity η_E. When applicable, this focuses the design freedom on linear viscoelastic properties, but this restricts independent control of key rheological phenomena. It is freeing, but more complex, when this connection is not applicable.

5. Ashby plots are useful but require significant data reduction to project function-valued properties into a low-dimensional space.

FUTURE ISSUES

1. Decoupled design of different rheological properties: τ, Ψ_1, η_E, η, etc.; what design freedom can exist for linear versus nonlinear behavior? Could constitutive models be superposed, and can this be related to multi-component microstructural design?
2. Engineering design and optimization methods can be applied to complex fluids. Surrogate modeling, sensitivity analysis, and optimization techniques exist that have not yet seen their full potential for rheological complexity.
3. Open access data repositories may significantly advance material selection for design with complex fluids, especially if coupled to visualization and learning techniques from data science. A challenge will be the high dimensionality of the data, including processing history effects, and advanced rheological characterization that is not yet standardized.
4. Design-driven organization of knowledge would benefit from more comparative studies of scaling laws for a given rheological design target, comparing a range of different microstructures. This will also more clearly reveal research needs, e.g. to identify quantitative front factors or where full simulation is necessary to relate structure to a desired property target.

DISCLOSURE STATEMENT

The authors are not aware of any biases that might be perceived as affecting the objectivity of this review.

ACKNOWLEDGMENTS

This work was supported in part by the Joint Center for Energy Storage Research (JCESR), an Energy Innovation Hub funded by the U.S. Department of Energy, Office of Science, Basic Energy Sciences, as well as the National Science Foundation under Grant No. CMMI-1463203 and No. CBET-1351342. We are similarly grateful to the Procter & Gamble Company, DuPont, and 3M for their support on the topic of rheology and design. CS would additionally like to acknowledge postdoctoral support from the Beckman Postdoctoral Fellows Program and the University of Illinois Urbana-Champaign. For helpful discussions on design and complex fluids, RHE thanks James T. Allison, Marco Caggioni, Jan Engmann, Jonathan B. Freund, William H. Hartt, A.E. (Peko) Hosoi, William P. King, Hector Lopez Hernandez, Christopher W. Macosko, Gareth H. McKinley, Florian Nettesheim, Vivek Sharma, Cliff Shin, and Jan Vermant, in addition to all members and collaborators of the Ewoldt Research Group that have contributed to such discussions, especially Rebecca E. Corman, Yong Hoon Lee, Arif Z. Nelson, and Jonathon K. Schuh.

LITERATURE CITED

Abed WM, Whalley RD, Dennis DJC, Poole RJ. 2016. Experimental investigation of the impact of elastic turbulence on heat transfer in a serpentine channel. *J. Nonnewton. Fluid Mech.* 231:68–78

Alves MA, Oliveira PJ, Pinho FT. 2021. Numerical Methods for Viscoelastic Fluid Flows. *Annu. Rev. Fluid Mech.* 53:509–41

Ash M, Ash I. 2006. *Handbook of Rheology Modifiers*. Endicott, NY: Synapse Information Resources, Inc.

Ashby MF. 2011. *Materials Selection in Mechanical Design*. Elsevier. 4th ed.

Astarita G, Marrucci G. 1974. *Principles of Non-Newtonian Fluid Mechanics*. McGraw-Hill Book Companies (UK)

Baird DG, Collias DI. 2014. *Polymer Processing: Principles and Design*. John Wiley & Sons

Barroso VC, Andrade RJ, Maia JM. 2010. An experimental study on the criteria for failure of polymer melts in uniaxial extension: The test case of a polyisobutylene melt in different deformation regimes. *J. Rheol. (N. Y. N. Y).* 54(3):605–18

Beavers GS, Joseph DD. 1975. The rotating rod viscometer. *J. Fluid Mech*. 69(3):475–511

Beiersdorfer P, Layne D, Magee EW, Katz JI. 2011. Viscoelastic Suppression of Gravity-Driven Counterflow Instability. *Phys. Rev. Lett.* 106(5):58301

Bergeron V, Bonn D, Martin JY, Vovelle L. 2000. Controlling droplet deposition with polymer additives. *Nature*. 405(6788):772–75

Beris AN, Tsamopoulos JA, Armstrong RC, Brown RA. 1985. Creeping Motion of a Sphere through a Bingham Plastic. *J. Fluid Mech.* 158:219–44

Berry GC, Fox TG. 1968. The viscosity of polymers and their concentrated solutions. In *Fortschritte Der Hochpolymeren-Forschung*, pp. 261–357. Springer

Bird RB. 1976. Useful non-Newtonian models. *Annu. Rev. Fluid Mech.* 8(1):13–34

Bird RB, Armstrong RC, Hassager O. 1987. *Dynamics of Polymeric Liquids: Volume 1 Fluid Mechanics*. John Wiley and Sons, Inc. 2nd ed.

Bird RB, Wiest JM. 1995. Constitutive equations for polymeric liquids. *Annu. Rev. Fluid Mech.* 27(1):169–93

Blackwell BC, Deetjen ME, Gaudio JE, Ewoldt RH. 2015. Sticking and splashing in yield-stress fluid drop impacts on coated surfaces. *Phys. Fluids*. 27(4):043101

Blaeser A, Duarte Campos DF, Puster U, Richtering W, Stevens MM, Fischer H. 2016. Controlling Shear Stress in 3D Bioprinting is a Key Factor to Balance Printing Resolution and Stem Cell Integrity. *Adv. Healthc. Mater.* 5(3):326–33

Bonn D, Denn MM, Berthier L, Divoux T, Manneville S. 2017. Yield stress materials in soft condensed matter. *Rev. Mod. Phys.* 89(3):35005

Braun DB, Rosen MR. 2000. *Rheology Modifiers Handbook: Practical Use and Application*. Norwich, New York: William Andrew Publishing

Bröckel U, Meier W, Wagner G, eds. 2013. *Product Design and Engineering: Formulation of Gels and Pastes*. Weinheim, Germany: Wiley-VCH

Burger ED, Munk WR, Wahl HA. 1982. Flow increase in the Trans Alaska Pipeline through use of a polymeric drag-reducing additive. *J. Pet. Technol.* 34(02):377–86

Carlson JD, Matthis W, Toscano JR. 2001. Smart prosthetics based on magnetorheological fluids. *Smart Struct. Mater. 2001 Ind. Commer. Appl. Smart Struct. Technol.*

Cates ME, Candau SJ. 1990. Statics and dynamics of worm-like surfactant micelles. *J. Phys.*

Condens. Matter. 2(33):6869
Chang EP. 1991. Viscoelastic windows of pressure-sensitive adhesives. *J. Adhes.* 34(1–4):189–200
Chaudhary G, Bharadwaj NA, Braun P V, Ewoldt RH. 2020. Exploiting Nonlinear Elasticity for Anomalous Magnetoresponsive Stiffening. *ACS Macro Lett.* 9(11):1632–37
Choueiri GH, Lopez JM, Hof B. 2018. Exceeding the asymptotic limit of polymer drag reduction. *Phys. Rev. Lett.* 120(12):124501
Christensen SF, McKinley GH. 1998. Rheological modelling of the peeling of pressure-sensitive adhesives and other elastomers. *Int. J. Adhes. Adhes.* 18(5):333–43
Clarke A, Howe AM, Mitchell J, Staniland J, Hawkes L, Leeper K. 2015. Mechanism of anomalously increased oil displacement with aqueous viscoelastic polymer solutions. *Soft Matter*. 11(18):3536–41
Clasen C, Phillips PM, Palangetic L, Vermant and J. 2012. Dispensing of rheologically complex fluids: the map of misery. *AIChE J.* 58(10):3242–55
Colombo J, Del Gado E. 2014. Stress localization, stiffening, and yielding in a model colloidal gel. *J. Rheol. (N. Y. N. Y).* 58(5):1089–1116
Considere PM. 1885. L'Emploi Du Fer Et De L'Acier: Dans Les Constructions. In *Annales Des Ponts et Chaussées. Mémoires et Documents Relatifs à l'art Des Constructions et Au Service de l'ingénieur*, Vol. 9, pp. 574–775
Corman RE. 2015. *Enabling Design with Rheological Complexity: Intuition and Optimization of Viscoelastic Materials*. University of Illinois at Urbana-Champaign
Corman RE. 2019. *Design Tools for Linear Viscoelastic Fluids*. University of Illinois at Urbana-Champaign
Corman RE, Ewoldt RH. 2019. Mapping linear viscoelasticity for design and tactile intuition. *Appl. Rheol.* 29(1):141–61
Corman RE, Rao L, Ashwin Bharadwaj N, Allison JT, Ewoldt RH. 2016. Setting material function design targets for linear viscoelastic materials and structures. *J. Mech. Des. Trans. ASME*. 138(5):1–12
Creton C, Ciccotti M. 2016. Fracture and adhesion of soft materials: a review. *Reports Prog. Phys.* 79(4):46601
Cussler EL, Moggridge GD. 2011. *Chemical Product Design*. Cambridge, UK: Cambridge University Press. 2nd ed.
D'Avino G, Greco F, Maffettone PL. 2017. Particle migration due to viscoelasticity of the suspending liquid and its relevance in microfluidic devices. *Annu. Rev. Fluid Mech.* 49:341–60
D'Avino G, Romeo G, Villone MM, Greco F, Netti PA, Maffettone PL. 2012. Single line particle focusing induced by viscoelasticity of the suspending liquid: theory, experiments and simulations to design a micropipe flow-focuser. *Lab Chip*. 12(9):1638–45
Dahlquist CA. 1969. Pressure-Sensitive Adhesives. In *Treatise on Adhesion and Adhesives*, ed. RL Patrick, p. 219. New York: Marcel Dekker
Dahlquist CA, Kolpe V V. 1974. Pressure-Sensitive Adhesives Comprising A Block Copolymer and a Tackifier. *US 3787531A*
de Gennes P-G. 1971. Reptation of a polymer chain in the presence of fixed obstacles. *J. Chem. Phys.* 55(2):572–79
de Gennes P-G. 1996. Soft adhesives. *Langmuir*. 12(19):4497–4500
Dealy JM. 2010. Weissenberg and Deborah numbers—their definition and use. *Rheol. Bull.*

79(2):14–18
Del Giudice F, D'Avino G, Greco F, Maffettone PL, Shen AQ. 2018. Fluid viscoelasticity drives self-assembly of particle trains in a straight microfluidic channel. *Phys. Rev. Appl.* 10(6):64058
Deplace F, Carelli C, Mariot S, Retsos H, Chateauminois A, et al. 2009. Fine tuning the adhesive properties of a soft nanostructured adhesive with rheological measurements. *J. Adhes.* 85(1):18–54
Derkach SR. 2009. Rheology of emulsions. *Adv. Colloid Interface Sci.* 151(1–2):1–23
Dobraszczyk BJ, Morgenstern MP. 2003. Rheology and the breadmaking process. *J. Cereal Sci.* 38(3):229–45
Dobrynin A V, Carrillo J-MY. 2011. Universality in nonlinear elasticity of biological and polymeric networks and gels. *Macromolecules*. 44(1):140–46
Espinosa-Garcia J, Lauga E, Zenit R. 2013. Fluid elasticity increases the locomotion of flexible swimmers. *Phys. Fluids*. 25(3):31701
Ewert TR, Mannion AM, Coughlin ML, Macosko CW, Bates FS. 2018. Influence of rheology on renewable pressure-sensitive adhesives from a triblock copolymer. *J. Rheol. (N. Y. N. Y).* 62(1):161–70
Ewoldt RH. 2014. Extremely Soft: Design with Rheologically Complex Fluids. *Soft Robot.* 1(1):12–20
Ewoldt RH, Clasen C, Hosoi AE, McKinley GH. 2007. Rheological fingerprinting of gastropod pedal mucus and synthetic complex fluids for biomimicking adhesive locomotion. *Soft Matter*. 3(5):634–43
Ewoldt RH, McKinley GH. 2017. Mapping thixo-elasto-visco-plastic behavior. *Rheol. Acta*. 56(3):195–210
Fielding SM. 2011. Criterion for extensional necking instability in polymeric fluids. *Phys. Rev. Lett.* 107(25):258301
Frazier S, Jiang X, Burton JC. 2020. How to make a giant bubble. *Phys. Rev. Fluids*. 5(1):13304
Freund JB, Kim J, Ewoldt RH. 2018. Field sensitivity of flow predictions to rheological parameters. *J. Nonnewton. Fluid Mech.* 257:71–82
Fulford GR, Katz DF, Powell RL. 1998. Swimming of spermatozoa in a linear viscoelastic fluid. *Biorheology*. 35(4–5):295–309
Gauzzelli E, Morris J. 2012. *A Physical Introduction to Suspension Dynamics*. Cambridge, UK: Cambridge University Press
Graham MD. 2014. Drag reduction and the dynamics of turbulence in simple and complex fluids. *Phys. Fluids*. 26(10):625–56
Graham MD. 2018. *Microhydrodynamics, Brownian Motion, and Complex Fluids*. Cambridge, UK: Cambridge University Press
Groisman A, Quake SR. 2004. A microfluidic rectifier: Anisotropic flow resistance at low Reynolds numbers. *Phys. Rev. Lett.* 92(9):3–6
Hagquist JAE, Hume III RM, Lund TL, Lund RI. Composition Inhibiting the Expansion of Fire, Suppressing Existing Fire, and Methods of Manufacture and Use Thereof. *US 7,163,642 B2*
Ho BP, Leal LG. 1976. Migration of rigid spheres in a two-dimensional unidirectional shear flow of a second-order fluid. *J. Fluid Mech.* 76(4):783–99
Holt SE, Perez MP. 2015. Impact Resistant, Torsion-Reducing Protective Athletic Gear Using Shear Thickening Fluid. *US 9,193,890 B2*
Hoyle DM, Fielding SM. 2016. Criteria for extensional necking instability in complex fluids and

soft solids. Part I: Imposed Hencky strain rate protocol. *J. Rheol. (N. Y. N. Y).* 60(6):1347–75
James DF. 2009. Boger fluids. *Annu. Rev. Fluid Mech.* 41:129–42
Jensen KE, Szabo P, Okkels F. 2012a. Topology optimization of viscoelastic rectifiers. *Appl. Phys. Lett.* 100(23):234102
Jensen KE, Szabo P, Okkels F, Alves MA. 2012b. Experimental characterisation of a novel viscoelastic rectifier design. *Biomicrofluidics*. 6(4):44112
Joseph DD. 1990. *Fluid Dynamics of Viscoelastic Liquids*. Springer-Verlag. Applied Ma ed.
Joshi YM, Denn MM. 2004. Failure and recovery of entangled polymer melts in elongational flow. *Rheol. Rev. 2004*. 1–17
Jossic L, Magnin A. 2001. Drag and stability of objects in a yield stress fluid. *AIChE J.* 47(12):2666–72
Kim B, Lee SS, Yoo TH, Kim S, Kim SY, et al. 2019. Normal stress difference–driven particle focusing in nanoparticle colloidal dispersion. *Sci. Adv.* 5(6):eaav4819
King GE. 2012. Hydraulic fracturing 101: What every representative, environmentalist, regulator, reporter, investor, university researcher, neighbor and engineer should know about estimating frac risk and improving frac performance in unconventional gas and oil wells. *SPE Hydraul. Fract. Technol. Conf.* Society of Petroleum Engineers
Kojic N, Bico J, Clasen C, McKinley GH. 2006. Ex vivo rheology of spider silk. *J. Exp. Biol.* 209(21):4355–62
Larson RG. 1999. *The Structure and Rheology of Complex Fluids*. New York: Oxford University Press
Larson RG, Desai PS. 2015a. Modeling the rheology of polymer melts and solutions. *Annu. Rev. Fluid Mech.* 47:47–65
Larson RG, Desai PS. 2015b. Modeling the Rheology of Polymer Melts and Solutions. *Annu. Rev. Fluid Mech.* 47:47–65
Larson RG, Wei Y. 2019. A review of thixotropy and its rheological modeling. *J. Rheol. (N. Y. N. Y).* 63(3):477–501
Lauga E. 2014. Locomotion in complex fluids: integral theorems. *Phys. Fluids*. 26(8):81902
Lauga E. 2016. Bacterial hydrodynamics. *Annu. Rev. Fluid Mech.* 48:105–30
Lee WK, Vaseleski RC, Metzner AB. 1974. Turbulent Drag Reduction in Polymeric Solutions Containing Suspended Fibers. *AIChE J.* 20(1):128–33
Lee YH, Schuh JK, Ewoldt RH, Allison JT. 2019. Simultaneous design of non-Newtonian lubricant and surface texture using surrogate-based multiobjective optimization. *Struct. Multidiscip. Optim.* 60(1):99–116
Leshansky AM, Bransky A, Korin N, Dinnar U. 2007. Tunable nonlinear viscoelastic "focusing" in a microfluidic device. *Phys. Rev. Lett.* 98(23):1–4
Li J, Mooney DJ. 2016. Designing hydrogels for controlled drug delivery. *Nat. Rev. Mater.* 1(12):1–17
Lin Y-J, Horner J, Illie B, Lynch ML, Furst EM, Wagner NJ. 2020. Molecular engineering of thixotropic, sprayable fluids with yield stress using associating polysaccharides. *J. Colloid Interface Sci.* 580:264–74
Lopez Hernandez H, Souza JW, Appel EA. 2020. A Quantitative Description for Designing the Extrudability of Shear-Thinning Physical Hydrogels. *Macromol. Biosci.* 2000295
Lumley JL. 1969. Drag reduction by additives. *Annu. Rev. Fluid Mech.* 1(1):367–84
M'barki A, Bocquet L, Stevenson A. 2017. Linking rheology and printability for dense and strong ceramics by direct ink writing. *Sci. Rep.* 7(1):1–10

Macosko CW. 1994. *Rheology Principles, Measurements, and Applications*. New York: Wiley-VCH
Martinetti L, Carey-De La Torre O, Schweizer KS, Ewoldt RH. 2018. Inferring the nonlinear mechanisms of a reversible network. *Macromolecules*. 51(21):8772–89
Martinetti L, Mannion AM, Voje Jr WE, Xie R, Ewoldt RH, et al. 2014. A critical gel fluid with high extensibility: The rheology of chewing gum. *J. Rheol. (N. Y. N. Y).* 58(4):821–38
McKinley GH, Hassager O. 1999. The Considère condition and rapid stretching of linear and branched polymer melts. *J. Rheol. (N. Y. N. Y).* 43(5):1195–1212
McKinley GH, Sridhar T. 2002. Filament-stretching rheometry of complex fluids. *Annu. Rev. Fluid Mech.* 34(1):375–415
Mewis J, Wagner NJ. 2009. Thixotropy. *Adv. Colloid Interface Sci.* 147:214–27
Mewis J, Wagner NJ. 2012. *Colloidal Suspension Rheology*. Cambridge, UK: Cambridge University Press
Moore F. 1959. The Rheology of Ceramic Slips and Bodies. *Trans. Br. Ceram. Soc.* 58:470–94
Morris JF. 2020. Shear thickening of concentrated suspensions: Recent developments and relation to other phenomena. *Annu. Rev. Fluid Mech.* 52:121–44
Mouritsen O, Styrbæk K. 2017. *Mouthfeel: How Texture Makes Taste*. New York: Columbia University Press
Münstedt H. 2018. Extensional rheology and processing of polymeric materials. *Int. Polym. Process.* 33(5):594–618
Nelson AZ. 2018. *Rheology and Design of Yield-Stress Fluids*. University of Illinois at Urbana-Champaign
Nelson AZ, Bras RE, Liu J, Ewoldt RH. 2018. Extending yield-stress fluid paradigms. *J. Rheol. (N. Y. N. Y).* 62(1):357–69
Nelson AZ, Ewoldt RH. 2017. Design of yield-stress fluids: A rheology-to-structure inverse problem. *Soft Matter*. 13(41):7578–94
Nelson AZ, Kundukad B, Wong WK, Khan SA, Doyle PS. 2020a. Embedded Droplet Printing in Yield-Stress Fluids. *Proc. Natl. Acad. Sci. U. S. A.* 117(11):5671–79
Nelson AZ, Kundukad B, Wong WK, Khan SA, Doyle PS. 2020b. Embedded droplet printing in yield-stress fluids. *Proc. Natl. Acad. Sci. U. S. A.* 117(11):5671–79
Nelson AZ, Schweizer KS, Rauzan BM, Nuzzo RG, Vermant J, Ewoldt RH. 2019. Designing and transforming yield-stress fluids. *Curr. Opin. Solid State Mater. Sci.* 23(5):100758
Nessil A, Larbi S, Belhaneche H, Malki M. 2013. Journal bearings lubrication aspect analysis using non-Newtonian fluids. *Adv. Tribol.* 2013:
Niu R, Ramaswamy M, Ness C, Shetty A, Cohen I. 2020. Tunable solidification of cornstarch under impact: How to make someone walking on cornstarch sink. *Sci. Adv.* 6(19):eaay6661
Nyström M, Qazi WM, Bülow M, Ekberg O, Stading M. 2015. Effects of Rheological Factors on Perceived Ease of Swallowing. *Appl. Rheol.* 25(6):9–17
O'Bryan CS, Bhattacharjee T, Hart S, Kabb CP, Schulze KD, et al. 2017. Self-assembled micro-organogels for 3D printing silicone structures. *Sci. Adv.* 3(5):
Olsen BD, Kornfield JA, Tirrell DA. 2010. Yielding Behavior in Injectable Hydrogels from Telechelic Proteins. *Macromolecules*. 43(21):9094–99
Owens MS, Vinjamur M, Scriven LE, Macosko CW. 2011. Misting of non-Newtonian liquids in forward roll coating. *J. Nonnewton. Fluid Mech.* 166(19–20):1123–28
Paschkewitz JS, Dubief Y, Shaqfeh ESG. 2005. The dynamic mechanism for turbulent drag reduction using rigid fibers based on Lagrangian conditional statistics. *Phys. Fluids*.

17(6):63102
Pek YS, WanAndrew CA, Shekaran A, Zhuo L, Ying JY. 2008. A thixotropic nanocomposite gel for three-dimensional cell culture. *Nat. Nanotechnol.* advanced o:
Pipkin AC. 1972. *Lectures on Viscoelasticity Theory*. New York: Springer
Poole RJ. 2012. The deborah and weissenberg numbers. *Rheol. Bull*. 53(2):32–39
Poole RJ, Budhiraja B, Cain AR, Scott PA. 2012. Emulsification using elastic turbulence. *J. Nonnewton. Fluid Mech.* 177:15–18
Puente-Velázquez JA, Godínez FA, Lauga E, Zenit R. 2019. Viscoelastic propulsion of a rotating dumbbell. *Microfluid. Nanofluidics*. 23(9):1–7
Rauzan BM, Nelson AZ, Lehman SE, Ewoldt RH, Nuzzo RG. 2018. Particle-Free Emulsions for 3D Printing Elastomers. *Adv. Funct. Mater.* 28(21):1707032
Read DJ, Auhl D, Das C, Den Doelder J, Kapnistos M, et al. 2011. Linking models of polymerization and dynamics to predict branched polymer structure and flow. *Science (80-.).* 333(6051):1871–74
Rodd LE, Cooper-White JJ, Boger D V., McKinley GH. 2007. Role of the elasticity number in the entry flow of dilute polymer solutions in micro-fabricated contraction geometries. *J. Nonnewton. Fluid Mech.* 143(2–3):170–91
Rodd LE, Scott TP, Boger D V, Cooper-White JJ, McKinley GH. 2005. The inertio-elastic planar entry flow of low-viscosity elastic fluids in micro-fabricated geometries. *J. Nonnewton. Fluid Mech.* 129(1):1–22
Roy A, Morozov A, van Saarloos W, Larson RG. 2006. Mechanism of polymer drag reduction using a low-dimensional model. *Phys. Rev. Lett.* 97(23):234501
Rubinstein M, Colby RH. 2003. *Polymer Physics*. Oxford, UK: Oxford University Press
Ruehs P, Bergfreund J, Bertsch P, Gstöhl S, Fischer P. 2021. Complex fluids in animal survival strategies. *Soft Matter*
Schuh JK, Ewoldt RH. 2019. Low Reynolds number friction reduction with polymers and textures. *J. Nonnewton. Fluid Mech.* 273:104167
Sen S, Morales AG, Ewoldt RH. 2020. Viscoplastic drop impact on thin films. *J. Fluid Mech.* 891:
Sharma SC, Yadav SK. 2014. Performance analysis of a fully textured hybrid circular thrust pad bearing system operating with non-Newtonian lubricant. *Tribol. Int.* 77:50–64
Sherman ZM, Howard MP, Lindquist BA, Jadrich RB, Truskett TM. 2020. Inverse methods for design of soft materials. *J. Chem. Phys.* 152(14):140902
Sousa PC, Pinho FT, Oliveira MSN, Alves MA. 2012. High performance microfluidic rectifiers for viscoelastic fluid flow. *RSC Adv.* 2(3):920–29
Spicer PT, Caggioni M, Squires TM. 2020. Complex Fluid Formulations: A Source of Inspiration and Innovation. *Chem. Eng. Prog.* 116(7):32–38
Steinberg V. 2021. Elastic Turbulence: An Experimental View on Inertialess Random Flow. *Annu. Rev. Fluid Mech.* 53:27–58
Stokes JR, Boehm MW, Baier SK. 2013. Oral processing, texture and mouthfeel: From rheology to tribology and beyond. *Curr. Opin. Colloid Interface Sci.* 18(4):349–59
Tabor M, De Gennes PG. 1986. A cascade theory of drag reduction. *EPL (Europhysics Lett.* 2(7):519
Tadmor Z, Bird RB. 1974. Rheological analysis of stabilizing forces in wire-coating dies. *Polym. Eng. Sci.* 14(2):124–36
Tanner RI. 1970. A theory of die-swell. *J. Polym. Sci. Part A-2 Polym. Phys.* 8(12):2067–78
Tanner RI. 2005. A theory of die-swell revisited. *J. Nonnewton. Fluid Mech.* 129(2):85–87

The International Organization for Standardization. 2021. ISO 16790:2021(en) Plastics — Determination of drawing characteristics of thermoplastics in the molten state

Tirtaatmadja V, McKinley GH, Cooper-White JJ. 2006. Drop formation and breakup of low viscosity elastic fluids: Effects of molecular weight and concentration. *Phys. fluids*. 18(4):43101

Tripathi A, Whittingstall P, McKinley GH. 2000. Using filament stretching rheometry to predict strand formation and "processability" in adhesives and other non-Newtonian fluids. *Rheol. Acta*. 39(4):321–37

Truby RL, Lewis JA. 2016. Printing soft matter in three dimensions. *Nature*. 540(7633):371–78

Tschoegl NW. 1989. *The Phenomenological Theory of Linear Viscoelastic Behavior: An Introduction*. Springer-Verlag

Ulrich KT, Eppinger SD, Yang MC. 2020. *Product Design and Development*. McGraw-Hill. seventh ed.

US Forest Service. 2020. Water Enhancers for Wildland Fire Management

van Vliet T. 2008. Strain hardening as an indicator of bread-making performance: a review with discussion. *J. Cereal Sci.* 48(1):1–9

Vasudevan M, Buse E, Lu D, Krishna H, Kalyanaraman R, et al. 2010. Irreversible nanogel formation in surfactant solutions by microporous flow. *Nat. Mater.* 9(5):436–41

Verbaan CAM, Peters GWM, Steinbuch M. 2017. The advantage of linear viscoelastic material behavior in passive damper design-with application in broad-banded resonance dampers for industrial high-precision motion stages. *J. Sound Vib.* 386:242–50

Verdier C, Piau J. 2003. Effect of nonlinear viscoelastic properties on tack. *J. Polym. Sci. Part B Polym. Phys.* 41(23):3139–49

Virk PS. 1975. Drag reduction fundamentals. *AIChE J.* 21(4):625–56

Virk PS, Mickley HS, Smith KA. 1970. The ultimate asymptote and mean flow structure in Toms' phenomenon. *J. Appl. Mech.* 37(2):488–93

Wagner NJ, Wetzel ED. 2010. Advanced body armor. *US7825045B1*

Wei M-H, Li B, David RLA, Jones SC, Sarohia V, et al. 2015a. Megasupramolecules for safer, cleaner fuel by end association of long telechelic polymers. *Science (80-.).* 350(6256):72–75

Wei TS, Fan FY, Helal A, Smith KC, McKinley GH, et al. 2015b. Biphasic Electrode Suspensions for Li-Ion Semi-solid Flow Cells with High Energy Density, Fast Charge Transport, and Low-Dissipation Flow. *Adv. Energy Mater.* 5(15):

White CM, Mungal MG. 2008. Mechanics and prediction of turbulent drag reduction with polymer additives. *Annu. Rev. Fluid Mech.* 40:235–56

Wijshoff H. 2010. The dynamics of the piezo inkjet printhead operation. *Phys. Rep.* 491(4–5):77–177

Wingstrand SL, Hassager O, Parisi D, Borger AL, Mortensen K. 2018. Flow induced crystallization prevents melt fracture of HDPE in uniaxial extensional flow. *J. Rheol. (N. Y. N. Y).* 62(4):1051–60

Witek DM, DOMBROWSKI R, WAGNER JN. 2020. Movement - Reactive Athletic Apparel and Methods of Making the Same. *US 2020/0345082 A1*

Xi L, Graham MD. 2012. Dynamics on the laminar-turbulent boundary and the origin of the maximum drag reduction asymptote. *Phys. Rev. Lett.* 108(2):28301

Yan C, Mackay ME, Czymmek K, Nagarkar RP, Schneider JP, Pochan DJ. 2012. Injectable solid peptide hydrogel as a cell carrier: effects of shear flow on hydrogels and cell payload. *Langmuir*. 28(14):6076–87

Yang S, Kim JY, Lee SJ, Lee SS, Kim JM. 2011. Sheathless elasto-inertial particle focusing and continuous separation in a straight rectangular microchannel. *Lab Chip*. 11(2):266–73

Yu AC, Hernandez HL, Kim AH, Stapleton LM, Brand RJ, et al. 2019. Wildfire prevention through prophylactic treatment of high-risk landscapes using viscoelastic retardant fluids. *Proc. Natl. Acad. Sci. U. S. A.* 116(42):20820–27

Zeitels SM, Hillman RE, Karajana-GI SS, Langer RS. 2011. Methods and Systems of Matching Voice Deficits with a Tunable Mucosal Implant to Restore and Enhance Individualized Human Sound and Voice Production. *WO 2011/109730 A2*

Zhu X, Wang S-Q. 2013. Mechanisms for different failure modes in startup uniaxial extension: Tensile (rupture-like) failure and necking. *J. Rheol. (N. Y. N. Y).* 57(1):223–48

TERMS AND DEFINITIONS

Rheology: the science of deformation and flow, particularly as applied to complex materials whose properties vary with time or applied deformation

Complex fluid: a fluid with non-Newtonian constitutive behavior

Design: an inverse problem wherein an objective is achieved by conceiving or constructing according to plan

Analysis: a forward problem to understand cause and effect

Viscoelastic: concurrent elastic energy storage and viscous energy dissipation

Relaxation modulus: in response to step input of shear strain γ_0, the observed (normalized) time-dependent shear stress response $G(t) \equiv \sigma(t)/\gamma_0$

Shear viscosity: the observed ratio of shear stress to shear strain rate, $\eta \equiv \sigma/\dot{\gamma}$, in simple shear flow defined by the velocity field $\underline{v} = \dot{\gamma} y \underline{e_x}$

Shear thinning: shear viscosity that decreases with flow strength (either stress or strain rate)

Thixotropy: time-dependent decrease of viscosity at high flow strength and subsequent time-dependent recovery at low flow strength

Yield-stress fluid: a flowable material that nevertheless behaves effectively as a solid below a critical yield stress

Shear thickening: shear viscosity that increases with flow strength

Normal stress in shear: in simple shear flow, the occurrence of non-zero stress differences $N_1 \equiv \sigma_{xx} - \sigma_{yy}$ and $N_2 \equiv \sigma_{yy} - \sigma_{zz}$, which define $\Psi_1 \equiv N_1 / \dot{\gamma}^2$ and $\Psi_2 \equiv N_2 / \dot{\gamma}^2$

Extensional viscosity: the observed ratio of tensile stress to extensional strain rate, $\eta_E \equiv T_{zz} / \dot{\varepsilon} = (\sigma_{zz} - \sigma_{xx}) / \dot{\varepsilon}$, in uniaxial elongation flow defined by the velocity field $\underline{v} = -\frac{1}{2}\dot{\varepsilon} x \underline{e_x} - \frac{1}{2}\dot{\varepsilon} y \underline{e_y} + \dot{\varepsilon} z \underline{e_z}$

Extensional thickening: extensional viscosity that increases with flow strength, or is larger than expected from shear viscosity, $\eta_E > 3\eta$

Material agnostic: insight that is independent of any chemistry or material microstructure details

Material specific: insight that is linked to particular chemistry or material-level physics

Ashby plot: named after Michael Ashby, a co-plot of two or more material properties, often used for material selection in design

Pipkin map: named after A. C. (Jack) Pipkin, the canonical map for graphically communicating distinctions between linear and nonlinear viscoelastic phenomena